

Elsevier Editorial System(tm) for Journal of  
Power Sources  
Manuscript Draft

Manuscript Number:

Title: Battery life estimation based on cloud data for electric vehicles

Article Type: Research Paper

Keywords: Electric vehicle; Cloud data; Battery pack capacity; Fuzzy control

Corresponding Author: Dr. Yuejiu Zheng, Ph.D.

Corresponding Author's Institution: University of Shanghai for Science and Technology

First Author: Kai Li

Order of Authors: Kai Li; Ping Zhou; Yifan Lu; Xuebing Han; Xiangjun Li; Yuejiu Zheng, Ph.D.

Manuscript Region of Origin: CHINA

**Abstract:** To evaluate the safety and life-cycle of electric vehicles (EVs), automobile companies usually retain the driving data of EVs on the cloud for monitoring and management. The recording period of the cloud data is generally as long as 10-30s at present, so the dynamic driving condition of EVs is hard to be revealed with the cloud data. But the charging data are stable, which makes it possible to estimate the battery life based on the charging cloud data. Battery life estimation includes capacity estimation and internal resistance estimation. In this paper, the capacity is directly estimated by the ampere hour integral method. The estimation results are modified based on the temperature data and optimized by the Kalman filter (KF). We further propose the Fuzzy logic (FL) to control the observation noise which effectively improves the accuracy of the estimation results. Then, the battery life is predicted by the Arrhenius empirical model. The sudden changes of voltage and current in the charging data are used for estimating the internal resistance. The internal resistance prediction is achieved using a similar process to the capacity prediction. The sampling test shows that the errors of the battery life estimation method are less than 4%.

Research Data Related to this Submission

---

There are no linked research data sets for this submission. The following reason is given:

The data that has been used is confidential

Dear Editor,

Enclosed is the manuscript by Kai LI and Yuejiu ZHENG titled "**Battery life estimation based on cloud data for electric vehicles**", which is being submitted for possible publication in Journal of Power Sources.

In recent years, with the increasing electric vehicle ownership, how to evaluate the performance of the power battery when it is applied in electric vehicles is a very important problem. We propose a method that can estimate the battery life of electric vehicles based on cloud data.

This research is supported by the International Science & Technology Cooperation of China under 2019YFE0100200, National Natural Science Foundation of China (NSFC) under the Grant number of 51877138, Shanghai Science and Technology Development Fund 19QA1406200 and the Science and Technology Foundation of State Grid Corporation of China (SGCC) under the contract number of DG71-19-024.

Authors of this paper are:

Kai Li, Ping Zhou, Yifan Lu, Xuebing Han, Xiangjun Li, Yuejiu Zheng.

The **first author** is Mr. **Kai LI**, the **corresponding author** is Dr. **Yuejiu ZHENG**.

The authors have complied with Elsevier's ethical requirements: Submission of an article implies that the work described has not been published previously, that it is not under consideration for publication elsewhere, that its publication is approved by all authors and tacitly or explicitly by the responsible authorities where the work was carried out. Submission also implies that, if accepted, it will not be published elsewhere in the same form, in English or in any other language, without the written consent of the Publisher.

Sincerely,

Yuejiu ZHENG

## Responses to Technical Check Results

<Journal of Power Sources>

<Battery life estimation based on cloud data for electric vehicles>

Dear Editor,

Thank you for your useful comments and suggestions on the language and structure of our manuscript. We have modified the manuscript accordingly, and detailed corrections are listed below point by point:

- 1) Please provide double line spacing in manuscript.

✓ We have changed the manuscript to double line spacing.

The manuscript has been resubmitted to your journal. We look forward to your positive response.

Sincerely,

Yuejiu ZHENG

# Battery life estimation based on cloud data for electric vehicles

Kai Li<sup>a</sup>, Ping Zhou<sup>a</sup>, Yifan Lu<sup>a</sup>, Xuebing Han<sup>b</sup>, Xiangjun Li<sup>c</sup>, Yuejiu Zheng<sup>a\*</sup>

<sup>a</sup> College of Mechanical Engineering, University of Shanghai for Science and Technology, Shanghai 200093, PR China.

<sup>b</sup> State Key Laboratory of Automotive Safety and Energy, Tsinghua University, Beijing 100084, PR China.

<sup>c</sup> Electrical Engineering and New Material Department, China Electric Power Research Institute, Beijing 100192, PR China

\*Correspondence to: [yuejiu.zheng@usst.edu.cn](mailto:yuejiu.zheng@usst.edu.cn) (Yuejiu Zheng)

**Abstract**—To evaluate the safety and life-cycle of electric vehicles (EVs), automobile companies usually retain the driving data of EVs on the cloud for monitoring and management. The recording period of the cloud data is generally as long as 10-30s at present, so the dynamic driving condition of EVs is hard to be revealed with the cloud data. But the charging data are stable, which makes it possible to estimate the battery life based on the charging cloud data. Battery life estimation includes capacity estimation and internal resistance estimation. In this paper, the capacity is directly estimated by the ampere hour integral method. The estimation results are modified based on the temperature data and optimized by the Kalman filter (KF). We further propose the Fuzzy logic (FL) to control the observation noise which effectively improves the accuracy of the estimation results. Then, the battery life is predicted by the Arrhenius empirical model. The sudden changes of voltage and current in the charging data are used for estimating the internal resistance. The internal resistance prediction is achieved using a similar process to the capacity prediction. The sampling test shows that the errors of the battery life estimation method are less than 4%.

**Key Words**—Electric vehicle; Cloud data; Battery pack capacity; Fuzzy control

## 1. Introduction

With the increasing power density and energy density of lithium-ion batteries, as well as its advantages such as high discharge rate and no memory effect, electric vehicles(EVs) with lithium-ion battery packs as power sources have received extensive attention[1,2]. The battery aging limits its energy storage and power output capability, as well as the performance of the EV including the cost and life span [3]. How to deal with the life management and asset evaluation of the power battery has become a key issue in the EV industry. In order to better detect and evaluate the performance of the power battery after it is applied in EVs, it is crucial to find an effective life estimation method for the battery pack.

Battery life estimation includes capacity estimation and internal resistance estimation. Capacity is an important indicator of battery state of health(SOH) estimation to evaluate the aging degree of the battery[4-6]. When the capacity degrades to a certain extent, the battery reaches the end of life (EOL) and cannot continue to work normally. Battery life estimation methods can be divided into empirical model-based and data-driven [7,8]. The empirical model-based method estimates and predicts the capacity using the experimental data. Because the general empirical model is an open-loop model, it is difficult to ensure the accuracy of the estimation results. The data-driven method typically involves establishing models to describe the battery degradation process[9-11], which can achieve higher estimation accuracy, but it is limited by the complexity of electrochemical modeling in real application[12]. Besides, the method generally requires certain working environment to estimate the battery life.

The internal resistance can be obtained by Electrochemical Impedance Spectroscopy (EIS) analysis[13], but this method is difficult to be applied with cloud data due to the low recording frequency[14]. The internal resistance can also be directly calculated by direct voltage response. In addition, there are methods based on electrochemical model, equivalent circuit model, neural network model[15-17], etc.

Advanced battery management using the cloud data has drawn interest in recent years. Li et al. [18] used vehicle cloud data combined with SDAE-ELM algorithm to establish a battery temperature model and proposed a new method for battery big data processing and quality evaluation. However, the model has not been tested in a wide range of temperature and the accuracy of the model needs to be improved. Tao et al. [19]established a scheduling model of EVs

on time dimension by comprehensively analyzing the data of 1,000 EVs on the cloud. By  
1  
2  
3  
4  
5  
6  
7  
8  
9  
10  
11  
12  
13  
14  
15  
16  
17  
18  
19  
20  
21  
22  
23  
24  
25  
26  
27  
28  
29  
30  
31  
32  
33  
34  
35  
36  
37  
38  
39  
40  
41  
42  
43  
44  
45  
46  
47  
48  
49  
50  
51  
52  
53  
54  
55  
56  
57  
58  
59  
60  
61  
62  
63  
64  
65  
analyzing the charging habits of users, they provided users with an orderly charging strategy to  
meet the user's demand for charging power. Michele et al. [20] put forward NCM-LMO capacity  
degradation model and analyzed 220 kinds of power battery capacity degradation based on cloud  
data from 16263 EVs. Due to the complexity of the driving condition of EVs, they made the  
model and EV driving data co-exist through some assumptions, which affected the accuracy of the  
model.

It is generally difficult to ensure the quality of the cloud data, which is a huge challenge to  
the model-based life estimation method. Although data are sampled with a high frequency in EVs,  
the recording period of the cloud data may be as long as 10-30s at present, because of the network  
bandwidth, and data storage capacity. As a result, the dynamic driving condition of EVs is hard to  
be revealed with the cloud data. But the charging data are stable compared to the dynamic driving  
condition, which makes it possible to estimate the battery life of EVs and provide prior knowledge  
for EVs of the same type and similar usage history.

Aiming at the problems mentioned above, a life estimation method for EVs battery pack  
based on cloud data is proposed in this paper. The capacity is directly estimated by the ampere  
hour integral method using a large amount of historical charging data. The estimation results are  
then modified based on the temperature data to obtain the preliminary capacity estimation results.  
Then the KF algorithm is used to optimize the estimation results, and the observation noise of KF  
algorithm is controlled by the FL algorithm in real time to improve the accuracy of estimation  
results. Based on the capacity estimation results, the battery life is predicted by the Arrhenius  
empirical aging model. The sudden changes of voltage and current in the charging data are used to  
estimate the internal resistance of the battery pack. The internal resistance prediction is achieved  
using a similar process to the capacity prediction. This method provides data support for  
preventive maintenance for battery packs, residual value assessment in EVs, and as well as the  
rapid classification before the secondary use.

The subsequent sections of this paper are arranged as follows: Section 2 and Section 3  
introduce the capacity and internal resistance estimation methods based on cloud data respectively.  
Section 4 presents the results and verification of the proposed methods. Section 5 summarizes the

proposed methods.

## 2. Capacity Estimation

Battery capacity is an important indicator for battery performance. The performance of Lithium-ion battery will gradually degrade under the influence of working environment and service time, which is manifested in the degradation of battery capacity and the increase of internal resistance [21]. Battery capacity usually shows a linear or exponential degradation law [22]. It is generally believed that when the current capacity of the battery degrades to 70% - 80% of the rated capacity, the battery reaches its end of life (EOL) [23,24].

SOH quantifies a battery's physical health condition compared with that of a fresh battery and is usually calculated by the capacity or impedance. In this paper, we define the SOH as the ratio of the current maximum available capacity to the rated capacity. The formula is as follows:

$$SOH = \frac{C_\alpha}{C_\beta} \times 100\% \quad (1)$$

where  $C_\alpha$  represents the current maximum available capacity,  $C_\beta$  represents the rated capacity of the battery [25].

Fig. 1(a) shows the flowchart of the capacity estimation.

- Step 1. The cloud data are preprocessed to obtain the current, voltage, state of charge (SOC), and mileage during the charge for capacity estimation.
- Step 2. The capacity is estimated preliminarily by the Ampere hour integral method; the result is represented by  $C_n$ .
- Step 3. Considering the effect of temperature, the  $C_n$  is modified according to the temperature data, and the result is represented by  $C_T$ .
- Step 4. The  $C_T$  is optimized with Kalman Filter based on Fuzzy Logic control (KF+FL) to obtain the final result of capacity estimation, and the result is represented by

$C_E$ .

- Step 5. The capacity are fitted and predicted by the Arrhenius empirical aging model, and the results are represented by  $C_P$ .

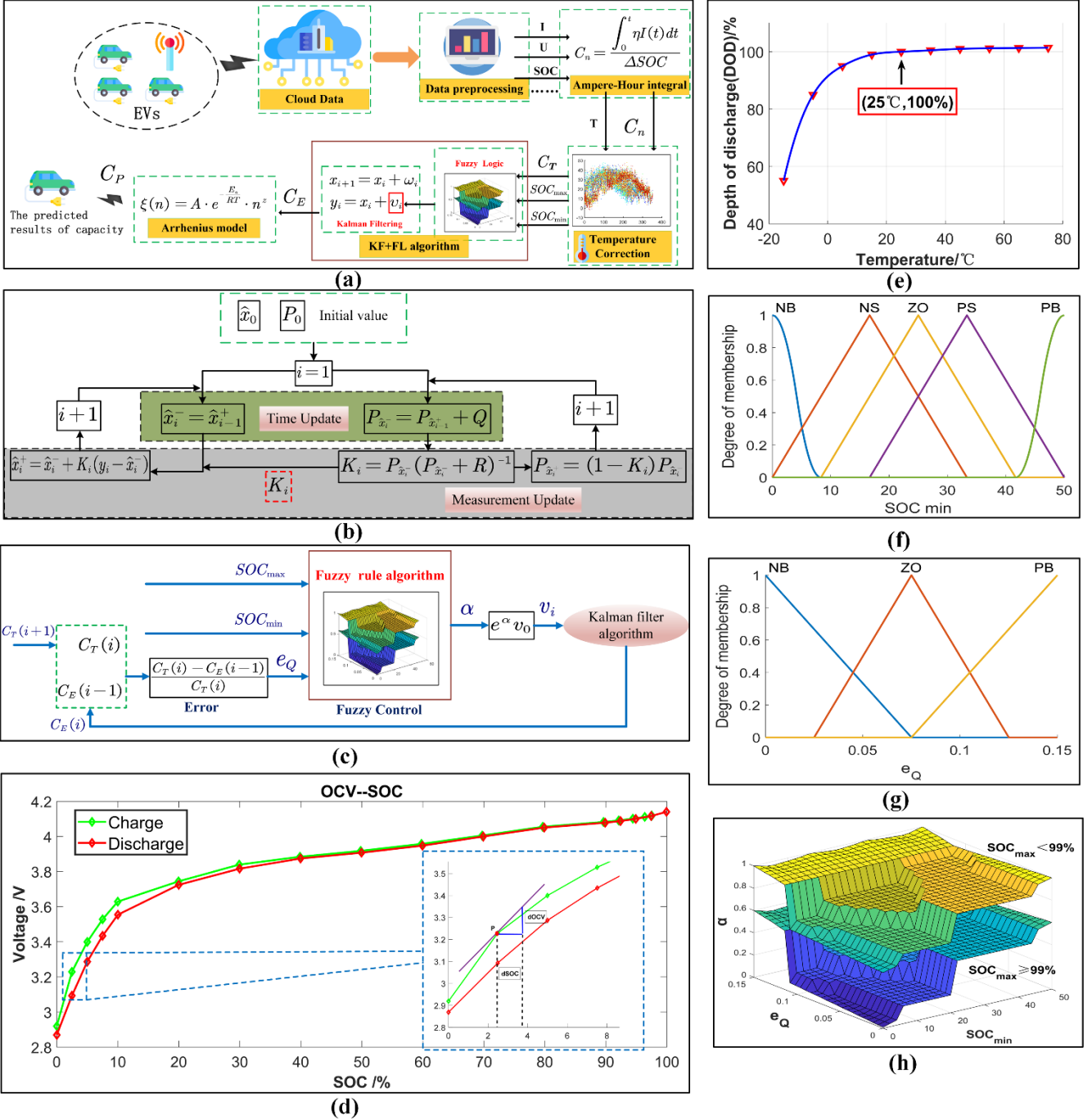


Fig. 1 (a)Capacity estimation process (b) KF algorithm process (c)KF+FL algorithm process (d)OCV-SOC curve (e)Relationship between depth of discharge and temperature (f) $SOC_{min}$  membership function (g) $e_Q$  membership function (h)Capacity fuzzy rule graph

## 2.1 Preliminary Estimation of Capacity

The ampere hour integral method is a common method. SOC is estimated by accumulating  
 1 the electric quantity during charge or discharge. If the start SOC of charge or discharge is  $SOC_0$ ,  
 2 then the current SOC is:  
 3  
 4

$$SOC = SOC_0 - \frac{1}{C_N} \int_0^t I(t) dt \quad (2)$$

where  $C_N$  represents the rated capacity,  $I(t)$  represents the current of the battery at time  $t$ .  
 11  
 12

Therefore, the ampere hour integral method can be used to estimate the capacity based on the  
 13 charging data. When estimating the capacity, the start SOC and end SOC of the  $i$ -th charging data  
 14 are recorded as  $SOC_{\min}$  and  $SOC_{\max}$  respectively, and  $\Delta SOC = SOC_{\max} - SOC_{\min}$ .  
 15  
 16  
 17  
 18  
 19  
 20  
 21  
 $Q_n(i)$  is the electric quantity changes in the  $i$ -th charging data. According to the capacity  
 22 calculation formula given in [26], the capacity  $C_n(i)$  can be obtained as follows:  
 23  
 24

$$C_n(i) = \frac{\int_{t_1}^{t_2} I(t) dt}{SOC_{\max} - SOC_{\min}} = \frac{Q_n(i)}{\Delta SOC} \quad (3)$$

where  $t_1$  represents the charging start time of the charging section,  $t_2$  represents the charging  
 31 end time of the charging section, and  $I(t)$  represents the current at time  $t$ .  
 32  
 33  
 34

## 38 2.2 Temperature Correction Method for Capacity

39 The lithium-ion battery under real vehicle driving condition will lead to changes in the  
 40 internal parameters of the battery due to different discharge rates and working environment.  
 41  
 42 Temperature is a factor that has a great influence on battery performance. When the lithium-ion  
 43 battery is working at a high-temperature environment, the reaction rate between the electrodes is  
 44 faster; when the working temperature is low, the lithium-ion activity is lower. The available  
 45 capacity and internal resistance of the battery will fluctuate greatly when the temperature changes  
 46  
 47 capacity and internal resistance of the battery will fluctuate greatly when the temperature changes  
 48 [27].  
 49  
 50

51 According to the temperature characteristic test of the battery, the discharge capacity of the  
 52 battery decreases obviously in the low-temperature environment and increases in the  
 53 high-temperature environment. Fig. 1(e) shows the relationship between depth of discharge (DOD)  
 54  
 55  
 56  
 57  
 58  
 59  
 60  
 61  
 62  
 63  
 64  
 65

and temperature, the depth of discharge of the battery is 100% at 25°C. Therefore, 25°C is set as  
 1 the standard temperature for temperature correction, and the  $C_n$  are corrected based on the  
 2 temperature data to obtain the standard capacity ( $C_T$ ).  
 3  
 4  
 5  
 6  
 7

### 8 2.3 Methods for Capacity Estimation and Prediction 9

10 KF algorithm is used to optimize the  $C_T$ , and the final capacity estimation result  $C_E$  is  
 11 obtained. Considering the slow change of battery capacity, when establishing EKF state equation,  
 12 it is considered that the capacity at time  $i+1$  is equal to that at time  $i$ . But there is system noise in  
 13 the model. The state equation for battery capacity is:  
 14  
 15  
 16  
 17  
 18

$$x_{i+1} = x_i + \omega_i \quad (4)$$

22 where  $x_i$  represents the optimal estimation capacity, and the system noise  $\omega_i$  satisfies the  
 23 filtering requirement by taking a smaller value due to the small variation of the capacity between  
 24 single charge intervals. The output equation is:  
 25  
 26  
 27

$$y_i = x_i + v_i \quad (5)$$

32 where  $y_i$  represents the capacity observation result ( $C_T$ ). Since  $C_T$  is the estimation result and  
 33 its error is different under different conditions, the observation noise  $v_i$  is set as a variable value.  
 34  
 35

36 In the process of capacity estimation, let  $v_i = e^\alpha v_0$ , where  $\alpha$  is determined by FL algorithm,  
 37 and  $v_0$  is the observation noise with the smallest observation error.  
 38  
 39

40 Fig. 1(b) shows the process of KF algorithm, which includes time update (prediction) and  
 41 measurement update (correction). In Fig. 1(b),  $\hat{x}_0$  and  $P_0$  are the initial values.  $\hat{x}_{i-1}^+$  is the  
 42 optimal estimation result of the previous state.  $\hat{x}_i^-$  is equal to the result of the previous state  
 43 estimation, and  $\hat{x}_i^+$  is the optimal estimation result of the current state.  $P_{\hat{x}_i^-}$  is the covariance  
 44 matrix of  $\hat{x}_i^-$ .  $P_{\hat{x}_{i-1}^+}$  is the covariance matrix of  $\hat{x}_{i-1}^+$ , and  $P_{\hat{x}_i^+}$  is the covariance matrix after  
 45 updating the current state.  $K_i$  is the current state Kalman Gain.  $Q$  and  $R$  are covariance  
 46  
 47  
 48  
 49  
 50  
 51  
 52  
 53  
 54  
 55  
 56  
 57  
 58  
 59  
 60  
 61  
 62  
 63  
 64  
 65

1           matrices of system noise  $\omega_i$  and observation noise  $v_i$ , respectively.  
2  
3  
4  
5  
6  
7  
8  
9  
10  
11  
12  
13  
14  
15  
16  
17  
18  
19  
20  
21  
22  
23  
24  
25  
26  
27  
28  
29  
30  
31  
32  
33  
34  
35  
36  
37  
38  
39  
40  
41  
42  
43  
44  
45  
46  
47  
48  
49  
50  
51  
52  
53  
54  
55  
56  
57  
58  
59  
60  
61  
62  
63  
64  
65

Fuzzy logic implements fuzzy comprehensive judgment by imitating the uncertainty concept judgment and reasoning thinking mode of the human brain, which includes three parts: fuzzification, fuzzy rule algorithm and defuzzification[28]. Fig. 1(c) shows the process of KF + FL algorithm,  $C_T(i)$  is the capacity observation of state  $i$ .  $C_E(i-1)$  is the capacity estimation result of state  $i-1$ , and the capacity estimation result  $C_E(i)$  is obtained through the KF + FL algorithm. The  $C_E(i)$  continues to participate in the filtering process of state  $i+1$ , improving the accuracy of capacity estimation with closed-loop correction.

The input parameters for the FL algorithm include  $SOC_{\min}$ ,  $SOC_{\max}$ , and relative error  $e_Q$  of capacity observations. As shown in formula (3),  $SOC_{\min}$  and  $SOC_{\max}$  have a great influence on the accuracy of battery capacity estimation results, so the estimation accuracy of SOC is an important factor to determine the observation noise  $v_i$  of KF algorithm. For example, when the battery is charged to the cut-off voltage, the battery management system (BMS) shows that the SOC of the battery is 100%, which has a high reliability. As a result, when  $SOC_{\max}$  approaches 100%,  $v_i$  is set to a small value. Fig. 1(d) shows the relationship between the open circuit voltage (OCV) and SOC, and the OCV drops faster in the low SOC range. When the BMS estimates the SOC, in the low SOC range, the  $dSOC/dOCV$  is smaller because the voltage drops faster. The SOC estimation result is often modified based on the voltage, and the SOC estimation result has a high reliability. Thus, when  $SOC_{\min}$  reaches a low SOC range,  $v_i$  can also be set to a small value. The error  $e_Q$  can represent the accuracy of the capacity observation. The smaller the error, the higher the accuracy. It also influences the output of the FL algorithm.

The main principle of the fuzzy rule is that the smaller  $SOC_{\min}$  and  $e_Q$ , the smaller  $\alpha$ . when any value of  $SOC_{\min}$  and  $e_Q$  is large,  $\alpha$  is large. Because the reliability of  $SOC_{\max}$  estimated by BMS decreases rapidly after it deviates from 100%, Binarization is used for  $SOC_{\max}$ . When  $SOC_{\max} \geq 99\%$ , the accuracy of SOC estimation result is higher. The fuzzy

rule graph in the lower part of Fig. 1(h) will be used. When  $SOC_{\max} < 99\%$  which means the accuracy of SOC estimation result is poor, the upper fuzzy rule chart in Fig. 1(h) is used to generate the coefficient  $\alpha$ . Because the SOC estimated by BMS has high precision in the low range and low precision in the middle range, the reliability of  $SOC_{\min}$  increases at a low SOC. This paper sets  $SOC_{\min} = 50\%$  as the boundary. When  $SOC_{\min} > 50\%$ , due to the low accuracy of SOC estimation, a larger  $v_i$  is set for KF algorithm. When  $0\% < SOC_{\min} < 50\%$ , fuzzy processing is performed for  $SOC_{\min}$ . The membership function is shown in Fig. 1(f), and the SOC is divided into five confidence intervals. From NB to PB, the reliability decreases in turn. A larger error  $e_Q$  indicates a low reliability of the capacity observation. In this paper, we set  $e_Q = 0.15$  as the boundary. When  $e_Q > 0.15$ , the reliability of the capacity observations is low, and a larger  $v_i$  is set directly for KF algorithm. When  $0 < e_Q \leq 0.15$ , fuzzy processing is performed for  $e_Q$ . The membership function is shown in Fig. 1(g).  $e_Q$  is divided into three confidence intervals. From NB to PB, the reliability decreases in turn. The output result  $\alpha$  of fuzzy processing for  $SOC_{\min}, SOC_{\max}$  and  $e_Q$  are shown in Fig. 1(h). The observation noise of KF algorithm  $v_i = e^\alpha v_0$  is controlled using the above FL algorithm.

Based on the capacity estimation results, battery life is predicted based on the Arrhenius empirical aging model. The Arrhenius empirical aging model formula is[29,30]:

$$\xi(n) = A \cdot e^{-\frac{E_a}{RT}} \cdot n^z \quad (6)$$

where  $\xi(n)$  is the relative capacity degradation after  $n$  cycles,  $A$  is the pre-exponential factor,  $E_a$  is the activation energy,  $R$  the gas constant,  $T$  the absolute temperature, and  $z$  is the exponent.

Since the temperature has been corrected to 25 °C during the capacity estimation process, the Arrhenius empirical aging model is simplified as follows:

$$\xi(n) = \eta \cdot n^z \quad (7)$$

where  $\eta$  is a constant, and  $n$  is time or mileage. There are two parameters ( $\eta$  and  $z$ ) need to be

1 identified using the estimation results. And then Equation (7) can be used to predict the remaining  
2 useful life.

### 3. Internal Resistance Estimation

7 The internal resistance of the battery is composed of the ohmic internal resistance and the  
8 polarization internal resistance. With the increase of cycles, the internal resistance of the battery  
9 increases gradually[31]. Fig. 2 (b) shows the relationship between the internal resistance and SOC  
10 at 25 °C. When  $SOC > 20\%$ , the internal resistance does not change much with the SOC.  
11  
12

13 When  $SOC < 20\%$ , the internal resistance increases significantly as the SOC decreases. It is  
14 mentioned in reference [32] that the battery has obvious polarization phenomenon at low  
15 temperature, and the polarization internal resistance increases, especially in the high SOC and low  
16 SOC ranges. Reference [33] shows that the ohmic internal resistance of the battery is stable and  
17 less affected by external environment when the lithium-ion battery SOC is between 30% and 80%  
18 and the operating temperature is constant.  
19  
20

21 Most of the charging process of EV battery pack is the multi-stage constant current charging.  
22 SOC at the current switching point is usually in the range of 50-80%. Thus, the internal resistance  
23 can basically represent the average level of the internal resistance of the battery. Therefore, this  
24 paper uses the voltage and current changes in the middle of the charging data to estimate the  
25 internal resistance of the battery pack.  
26  
27

28 Fig. 2 (a) shows the flowchart of the internal resistance estimation.  
29  
30

- 31     ● Step 1. The current, voltage, SOC and other data are obtained by preprocessing the  
32         cloud data.  
33  
34     ● Step 2. The charging data are analyzed to estimate the internal resistance. As shown in  
35         Fig. 2 (g), the charging process of battery pack is mostly the multi-stage constant current  
36         charging. The internal resistance can be estimated by the current difference and voltage  
37         difference generated during two charging mode.  
38  
39     ● Step 3. The preliminary internal resistance estimation result is represented by  $r$ , which  
40         is further corrected to be  $r_T$  based on the temperature data.  
41  
42  
43  
44  
45  
46  
47  
48  
49  
50  
51  
52  
53  
54  
55  
56  
57  
58  
59  
60  
61  
62  
63  
64  
65

- Step 4. The KF + FL algorithm is used to optimize  $r_T$  to get the final estimation result of internal resistance( $r_E$ ).
- Step 5. The internal resistance is predicted based on the linear model.

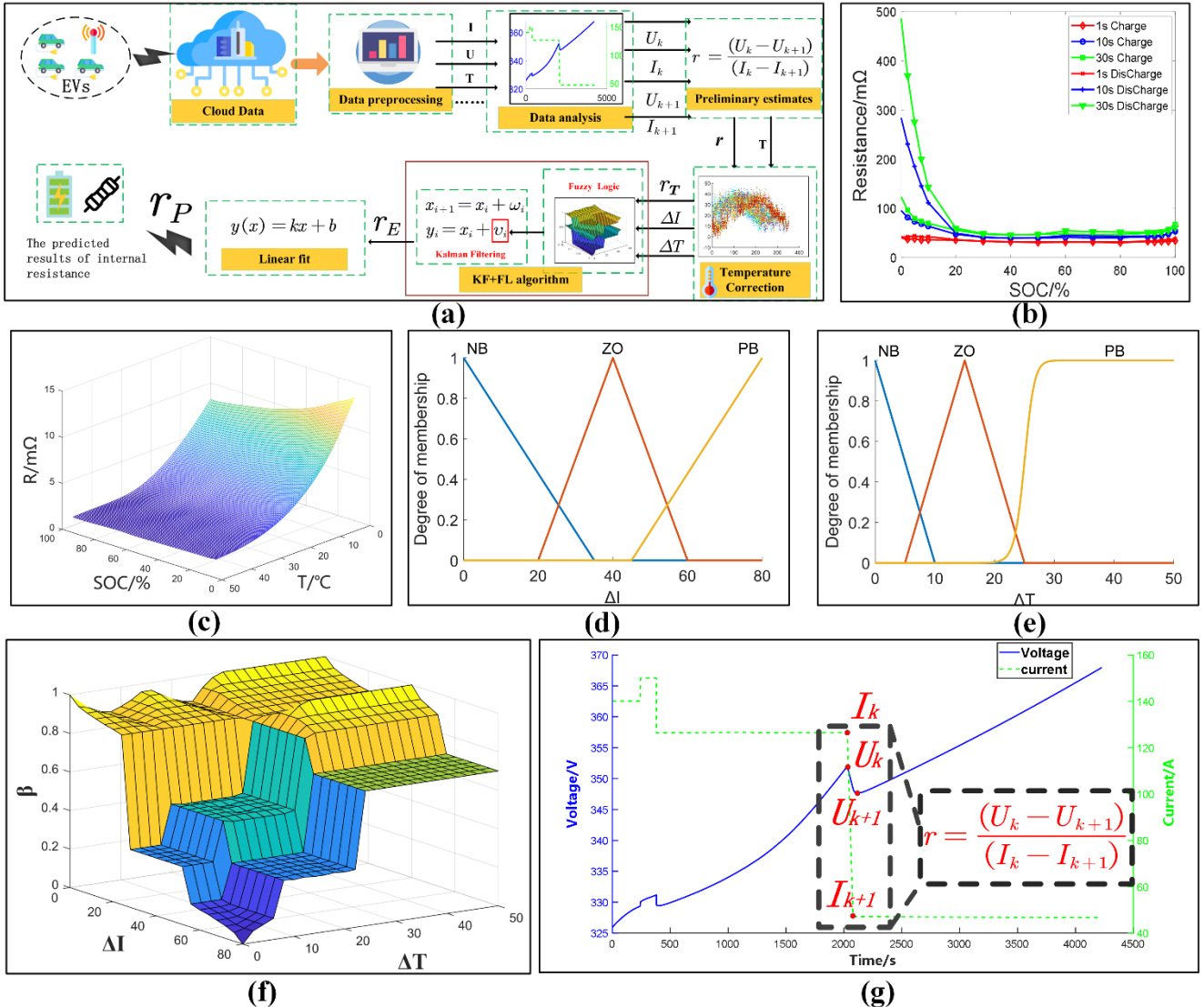


Fig. 2 (a)Internal resistance estimation process (b)Relationship between internal resistance and SOC under different charging and discharging pulses (c)Relationship between internal resistance, temperature and SOC (d) $\Delta I$  membership function (e) $\Delta T$  membership function (f)internal resistance fuzzy rule graph (g)Charging voltage and current

### 3.1 Preliminary Estimation of Internal Resistance

As shown in Fig. 2 (g), the time tick  $k$  is firstly found with current change in the middle of charging data by processing the cloud data.  $I_k$  and  $U_k$  are the current and voltage at time tick  $k$  respectively.  $I_{k+1}$  and  $U_{k+1}$  are the current and voltage at time tick  $k+1$  respectively. The

internal resistance is calculated by the ratio of voltage difference to current difference before and after the current change as shown in formula (8).

$$r = \frac{U_k - U_{k+1}}{I_k - I_{k+1}} \quad (8)$$

### 3.2 Temperature Correction Method for Internal Resistance

Fig. 2 (c) shows the map describing the relationship between internal resistance, temperature and SOC. Temperature has a great influence on the internal resistance of the battery, and the internal resistance increases rapidly in low temperature environment.  $r_T$  is achieved by modifying  $r$  according to the temperature data and the map.

### 3.3 Methods for Internal Resistance Estimation and Prediction

The KF+FL algorithm is used to optimize the  $r_T$ , and the final internal resistance estimation result  $r_E$  is obtained. The EKF state equation, which is the same as formula (4)-(5), is established also because of the small change of internal resistance in the single charge interval. The observation noise  $v_i$  is set as a variable value. In the process of internal resistance estimation, we set  $v_i = e^\beta v_0$ , where  $\beta$  is determined by FL algorithm, and  $v_0$  is the observation noise with the smallest observation error.

The input parameters for the FL algorithm include current difference ( $\Delta I$ ) and temperature difference ( $\Delta T$ ), where  $\Delta I = I_k - I_{k+1}$ ,  $\Delta T = T_k - 25^\circ\text{C}$ . According to formula (8), the current has a great influence on the internal resistance estimation results. If  $\Delta I$  is small, the internal resistance estimation results will be larger. Therefore,  $\Delta I$  is selected as the input parameter of FL algorithm. It can be seen from Fig. 2(c) that the temperature has a great influence on the internal resistance of the battery. A large  $\Delta T$  will lead to a large difference in the internal resistance estimation results. Therefore,  $\Delta T$  is selected as the input parameter of FL algorithm.

The main principle of the fuzzy rule is that when  $\Delta I$  is larger and  $\Delta T$  is smaller,  $\beta$  is smaller. According to the process of the FL algorithm,  $\Delta I$  and  $\Delta T$  are fuzzified into three

confidence intervals as shown in Fig. 2(d) and (e). The output result  $\beta$  is shown in Fig. 2(f). The observation noise of KF algorithm  $v_i = e^\beta v_0$  is controlled using the above FL algorithm.

Based on the internal resistance estimation results, the internal resistance is predicted using the simple linear model:

$$y(x) = kx + b \quad (9)$$

where  $k$  and  $b$  are parameters which need to be identified using the estimation results;  $x$  is time or mileage, and  $y(x)$  is the prediction result.

## 4. Experiment and Verification with Real Vehicle Data

### 4.1 Real Vehicle Data Overview

A total of 147 vehicle data provided by data sources A and B are obtained for real vehicle data verification. The data characteristics are shown in Table 1. These data are all processed using the open source language Python.

**Table 1**

Basic Information of Real Vehicle Data

Source	Number of data	Sampling days
A	47	~345
B	100	~469

Data source A provides cloud data of 47 EVs in total, with the maximum data sampling days of 345 days. The data sampling interval is 30s, and the data content includes vehicle data (vehicle speed, mileage, motor speed, etc.) and power battery data (total current, total voltage, SOC, temperature, etc.). There is no cell voltage data. Only the extreme value data of cell voltage is observed in the data. Data source B provides cloud data of 100 EVs in total, with the maximum data sampling days of 469 days. The data sampling interval is 1s, and the data content includes vehicle data (vehicle speed, mileage, motor speed, etc.) and power battery data (total current, total voltage, SOC, temperature, etc.), including all cell voltage data.

To show an overview of the data, an EV in data source A is randomly selected and displayed. The EV has been running for 315 days, and 319 charges are obtained from the cloud data of the

EV. Fig. 3(a) shows the charging time and the depth of charge (DOC)  $\Delta SOC$  of the 319 charges. Fig. 3(b) shows the frequency distribution histogram of the charging time, and the red curve is the probability density curve. 95% of the charging time of the EV is distributed within 0 to 2 hours, with an average of 1.7 hours. Fig. 3 (c) shows the  $\Delta SOC$  distribution of 319 charges, with an average DOC of 41%. The DOC is mostly concentrated in the range of 40% to 60%, and the overall distribution decreases from the middle to both sides. Fig. 3 (d) shows the start of charge ( $SOC_{min}$ ) distribution of 319 charges. Fig. 3 (e) shows the end of charge ( $SOC_{max}$ ) distribution of 319 charges. The start of charge is mainly from 30%-50%, and there is a large part for the end of charge is larger than 90%. The temperature data of the EV is shown in Fig. 3 (f). The maximum temperature difference during the operation of the EV is 43°C.

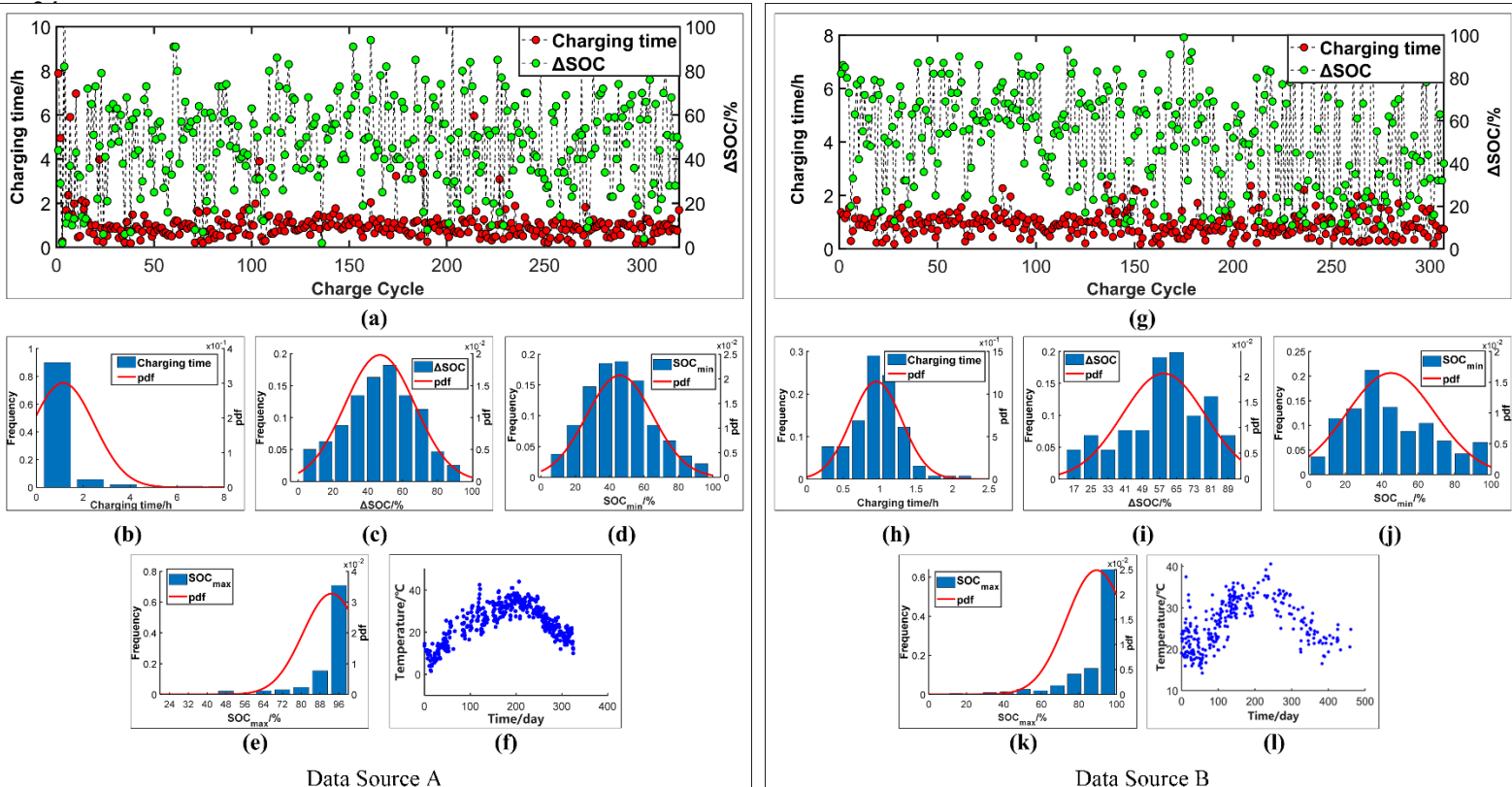


Fig. 3 (a) and (g) charging time and depth of charge  $\Delta SOC$  (b) and (h) frequency distribution histogram of the charging time (c) and (i) frequency distribution histogram of  $\Delta SOC$  (d) and (j) frequency distribution histogram of  $SOC_{min}$  (e) and (k) frequency distribution histogram of  $SOC_{max}$  (f) and (l) Temperature data

In data source B, the cloud data of one EV is also randomly selected and displayed. The EV has been running for 416 days, and 307 charges are obtained from the cloud data of the EV. Fig. 3

(g) shows the charging time and  $\Delta SOC$  of 307 charges. Fig. 3(h) shows the frequency distribution histogram of the charging time, and the red curve is the probability density curve. The average charging time of the EV is 0.95 hours, which is much faster than the EV in data source A. Fig. 3(i) shows the  $\Delta SOC$  distribution of 307 charges, with an average DOC of 59%. The DOC is mostly concentrated in the range of 60% to 80%. Compared to the EV in data source A, the DOC is deeper. Fig. 3(j) and (k) shows  $SOC_{min}$  and  $SOC_{max}$  distribution of 307 charges, respectively. The start of charge is mainly from 10%-50%, and there is also a large part for the end of charge is larger than 90%. The temperature data of the EV is shown in Fig. 3(l). The maximum temperature difference during the operation of the EV is 27°C.

## 4.2 Results of capacity estimation and prediction

One of the vehicles is randomly extracted from data source A to show an example for the capacity estimation and prediction. The capacity is estimated by the method in Section 2, and the preliminary estimation results are shown in Fig. 4(a). The blue cross points represent the capacity estimation results directly obtained from the ratio of  $Q_n$  and  $\Delta SOC$ . Although the degradation trend of the battery is obvious, the estimation results are unstable and some of the errors are large, which makes the regularity of the overall estimation result poor. The red circular points in Fig. 4(a) represent the  $C_T$ . After considering the effect of temperature on the results of the capacity estimation, the results of the low temperature interval capacity estimation increase, and the results of the high temperature interval capacity estimation decrease, which makes the estimation result closer to the true value.

Fig. 4(b) shows the results of  $C_T$  optimization with KF algorithm and KF + FL algorithm respectively, and the blue circular points represent the results of  $C_T$  optimization with KF algorithm. The initial values of the KF algorithm are as follows:  $\hat{x}_0 = 130Ah$ ,  $P_0 = 1$ ,  $Q = 0.03^2$ ,  $R = 0.05^2$ . Although the estimation results tend to converge, the capacity estimation results cannot converge due to the large errors of some  $C_T$  values. The black circular

1 points represent the results of  $C_T$  optimization with KF+FL algorithm. The initial values of the  
 2 KF+FL algorithm are as follows:  $\hat{x}_0 = 130Ah$ ,  $P_0 = 1$ ,  $Q = 0.03^2$ .  $R$  is controlled in real  
 3 time by the FL algorithm introduced in section 2.3. The results show that although there are some  
 4 estimation errors in  $C_T$ , the capacity estimation results can be converged by controlling the  
 5 weight of  $C_T$  in real time with FL algorithm, and accord with the real degradation trend of  
 6 power battery capacity. An advantage of the KF+FL algorithm is that the initial capacity is not  
 7 critical as the estimation result will converge to the true value. The red circular points in Fig. 4(b)  
 8 represent the capacity estimation results when the KF + FL algorithm is set to  
 9  $\hat{x}_0 = C_0 = 110Ah$ . Although the initial value of the algorithm is quite different from the true  
 10 value, the algorithm can still correct the result to the true value.  
 11

12 The battery capacity of the EV is predicted based on the Arrhenius empirical aging model.  
 13 The prediction results are shown in Fig. 4(c), where the red points represent the capacity  
 14 estimation results. The green curve represents the prediction curve based on  $C_E$  using the  
 15 Arrhenius empirical aging model, and the prediction interval is 315 days to 700 days. The blue  
 16 points represent the predicted capacity of the battery on the 700th day after use.  
 17

1  
 2  
 3  
 4  
 5  
 6  
 7  
 8  
 9  
 10  
 11  
 12  
 13  
 14  
 15  
 16  
 17  
 18  
 19  
 20  
 21  
 22  
 23  
 24  
 25  
 26  
 27  
 28  
 29  
 30  
 31  
 32  
 33  
 34  
 35  
 36  
 37  
 38  
 39  
 40  
 41  
 42  
 43  
 44  
 45  
 46  
 47  
 48  
 49  
 50  
 51  
 52  
 53  
 54  
 55  
 56  
 57  
 58  
 59  
 60  
 61  
 62  
 63  
 64  
 65

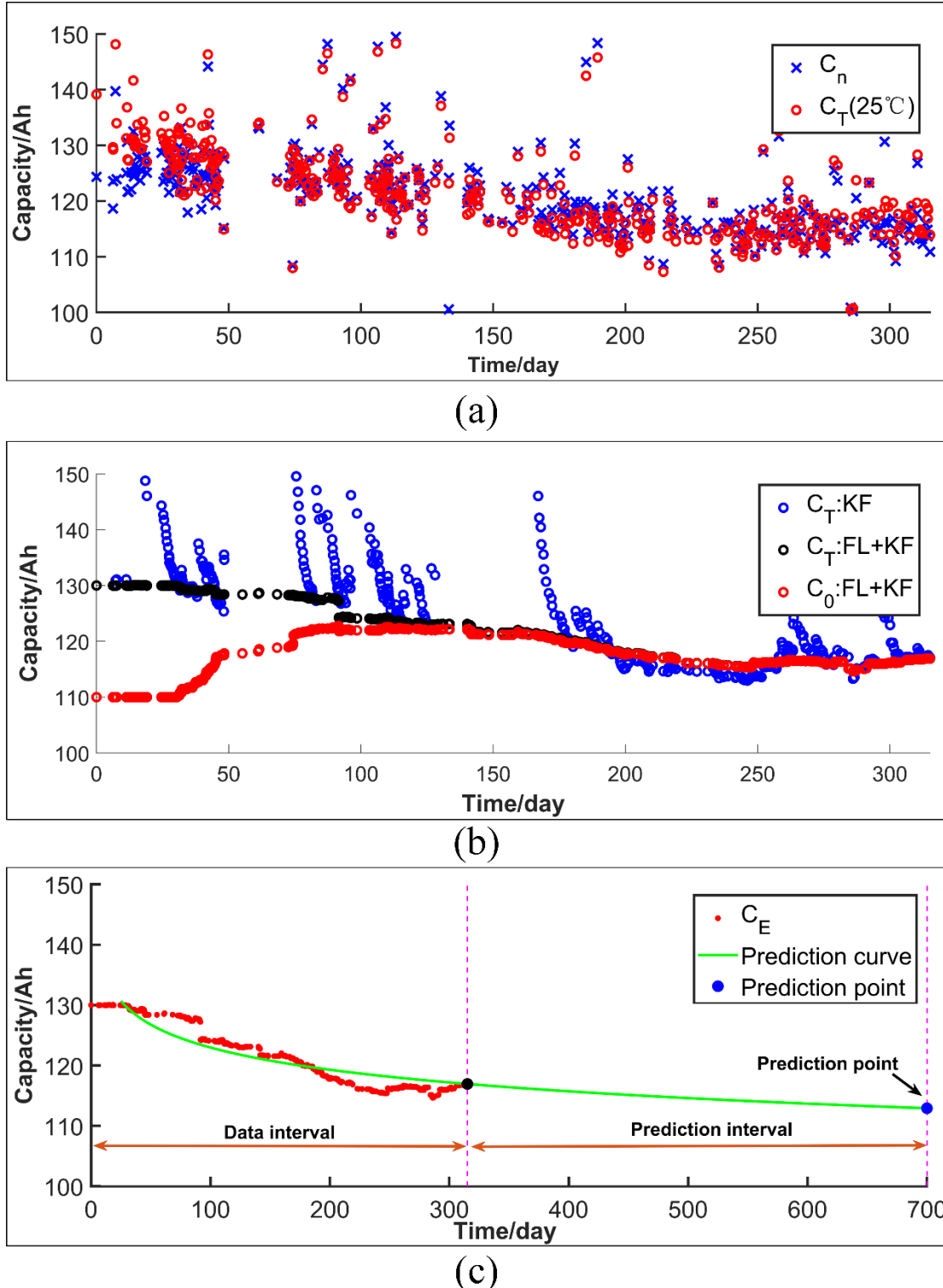


Fig. 4 (a) Preliminary capacity estimation results (b)Capacity estimation results of KF Algorithm and KF + FL Algorithm (c) Capacity Prediction results

Fig. 5 shows the capacity estimation results for all EVs provided by data source A. Fig. 5 (a) shows the  $C_n$ , where the points of the same color represent the capacity estimation results of the same EV. It can be seen from the preliminary estimation results that due to the huge and complex

cloud data, some of the capacity estimation results have large errors, but most of the estimation results are accurate. The degradation trend of power battery capacity can be observed, which provides the basis for capacity estimation. Fig. 5 (b) shows the temperature data of 47 EVs, where the points of the same color represent the temperature data of the same EV.

Fig. 5(c) shows the  $C_T$ . Due to the large amount of data, the effect of temperature correction cannot be clearly displayed in Fig. 5(c). Therefore, four EVs are randomly selected from 47 EVs. The estimated results before and after the temperature correction of these four EVs are shown in Fig. 5(e). The blue points represent  $C_n$ , and the orange points represent  $C_T$ . Fig. 5(d) shows the  $C_E$  obtained by the KF + FL algorithm. The initial values of KF + FL algorithm are set as follows:  $\hat{x}_0 = 130Ah$ ,  $P_0 = 1$ ,  $Q = 0.03^2$ .

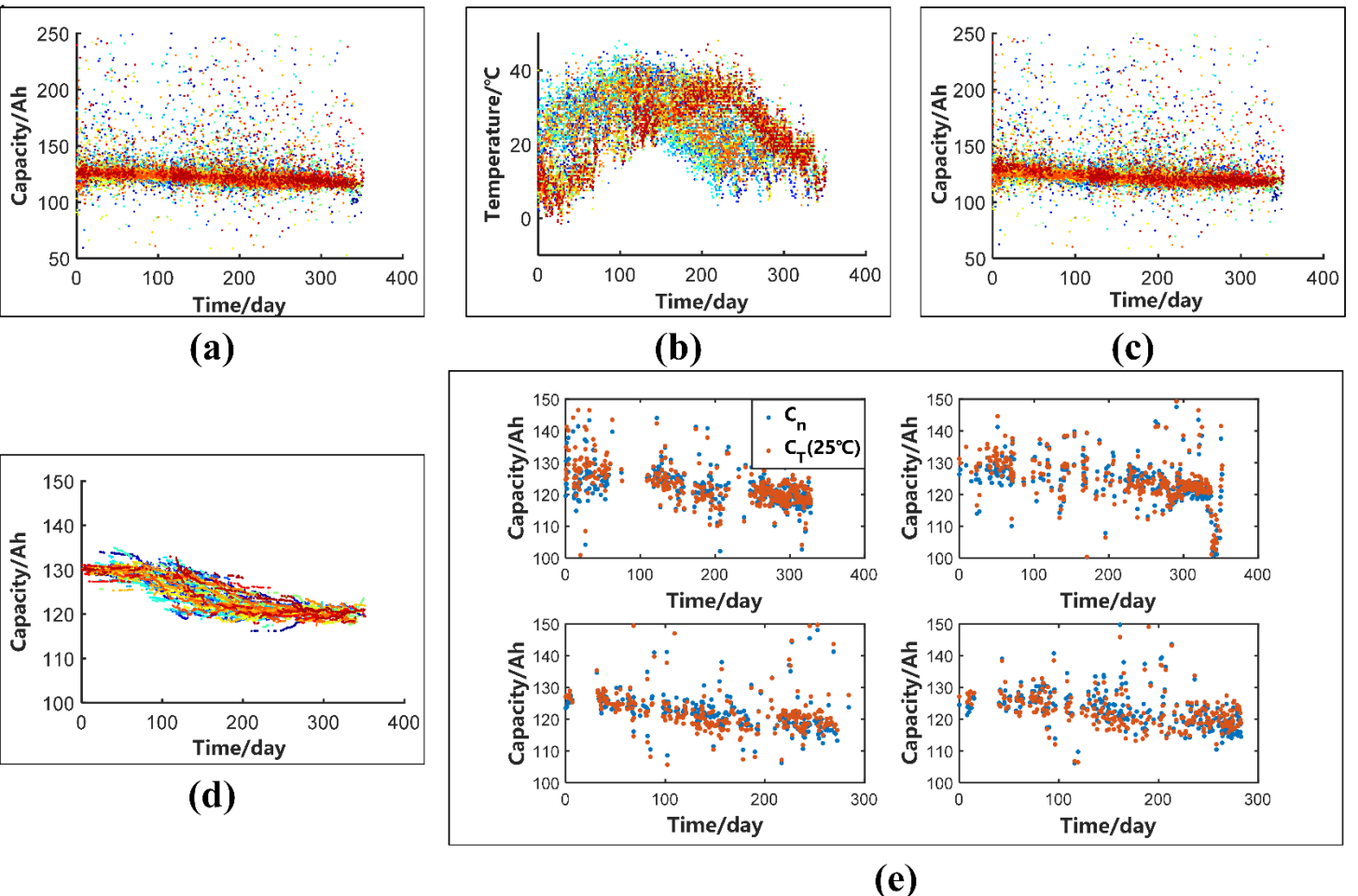
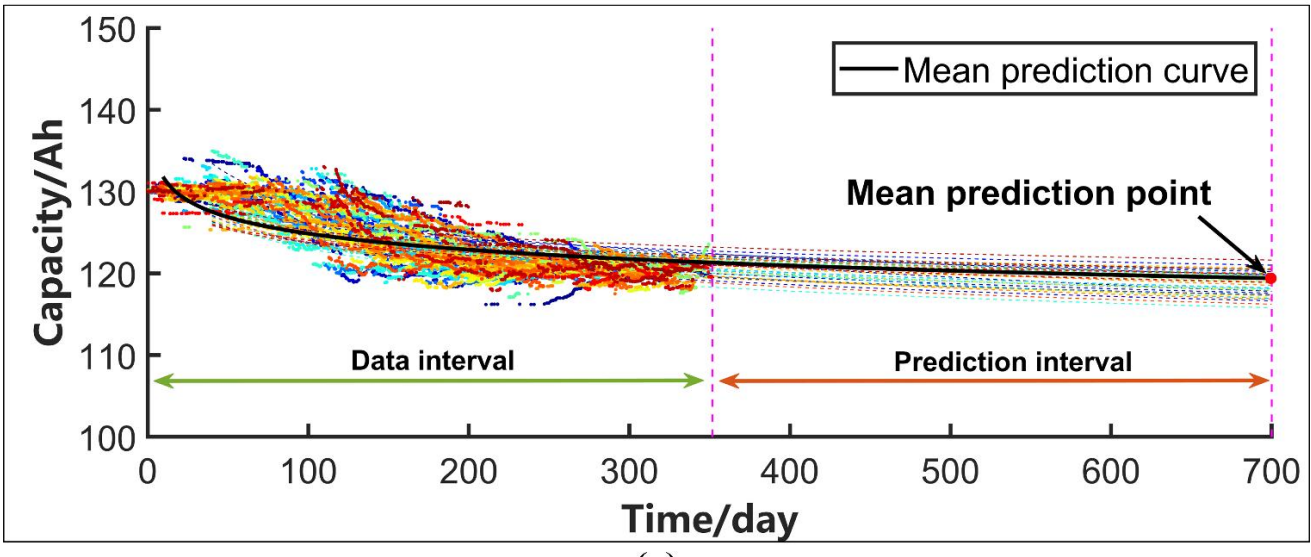


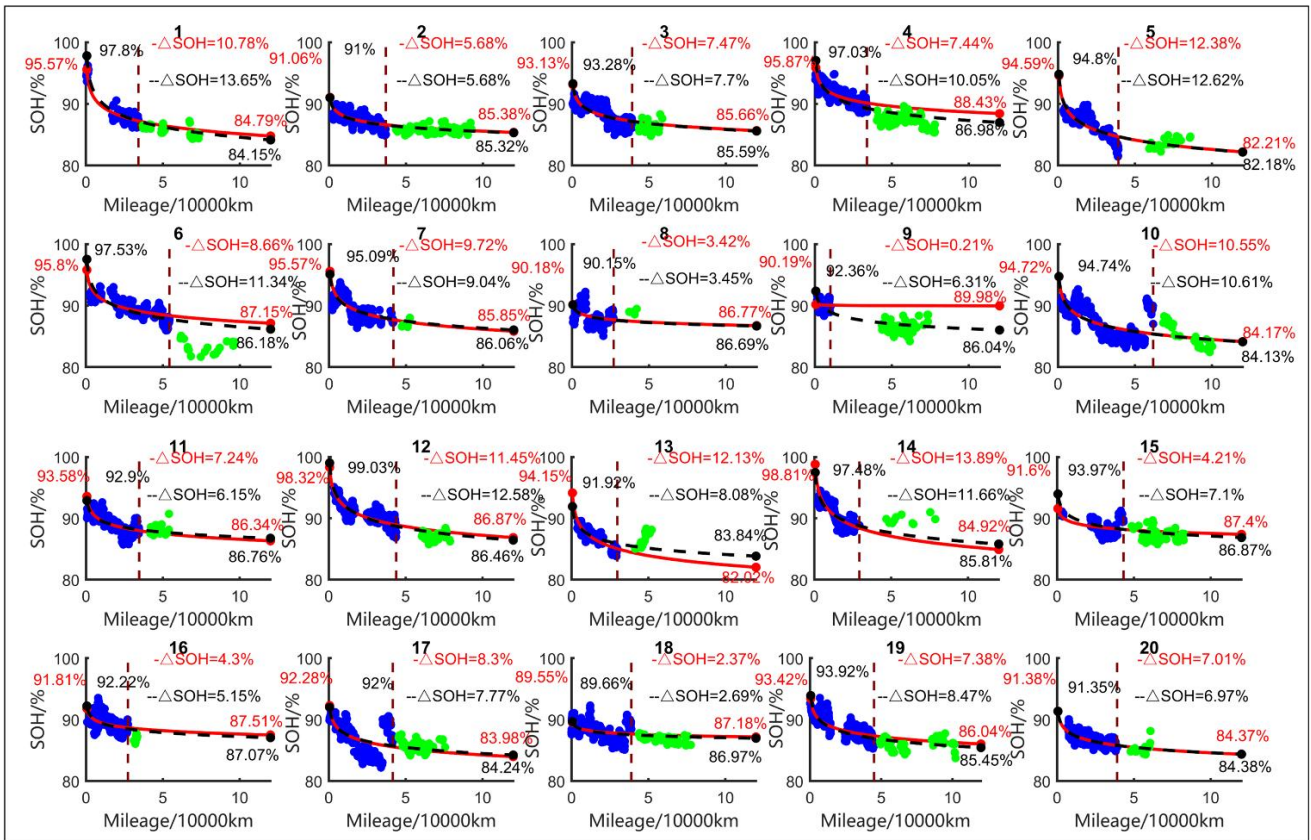
Fig. 5 All EVs from data source A: (a) Preliminary capacity estimation results (b) Temperature data (c) Temperature correction results (d) Capacity estimation results of KF + FL Algorithm (e) Single EV temperature correction results

1 Based on the capacity estimation results, the capacity of 47 EVs provided by data source A is  
2 predicted based on the Arrhenius empirical aging model. The prediction results are shown in Fig.  
3  
4 6 (a). The dotted lines represent the capacity prediction results of each EV, the black solid line  
5 represents the average prediction result of all EVs, and the red dot represents the mean predicted  
6 capacity at the 700th day.  
7

8  
9 The estimation results of 20 EVs in data source B are shown in Fig. 6 (b). Considering that  
10 different EVs have been put into operation successively at the beginning of data recording, the  
11 SOH corresponding to zero mileage is not 100%. Besides, data source B is divided into two  
12 sections  $B_1$  and  $B_2$  in order to have a preliminary verification from data to data.  
13  
14  
15  
16  
17  
18  
19  
20  
21  
22  
23  
24  
25  
26  
27  
28  
29  
30  
31  
32  
33  
34  
35  
36  
37  
38  
39  
40  
41  
42  
43  
44  
45  
46  
47  
48  
49  
50  
51  
52  
53  
54  
55  
56  
57  
58  
59  
60  
61  
62  
63  
64  
65



(a)



(b)

Fig. 6 (a)Capacity prediction results of 47 EVs (b) Model free SOH estimation and empirical life model SOH prediction based on EV cloud data

The blue points in Fig. 6 (b) represent the SOH estimation results ( $S_E(B_1)$ ) based on data  $B_1$ . The brown vertical line is the driving mileage of each EV in data  $B_1$ , and the driving mileage of most EVs is between 20000 km and 60000 km, mostly 40000 km. The  $S_E(B_1)$  are

fitted based on the Arrhenius empirical aging model to obtain a red prediction curve. Further, data  
 1  
 $B_2$  is used for verifying the SOH estimation results based on data  $B_1$ . The green points  
 2  
 represent the SOH estimation results ( $S_E(B_2)$ ) obtained based on data  $B_2$ . It can be seen that  
 3  
 $S_E(B_2)$  fluctuates near the red prediction curve. The estimation results can converge to the  
 4  
 prediction curve, which shows that the method itself is reliable. The black dotted line represents  
 5  
 the prediction curve obtained based on all data ( $B_1 + B_2$ ). EVs numbered 7, 8, 13 and 20 are  
 6  
 less used during data  $B_2$ , which means the verification from data to data for these EVs has less  
 7  
 significance. The 9th EV is less used in data  $B_1$ , so the two prediction results are very different.  
 8  
 For the other EVs, the black dotted lines coincide with the red curves well, which indicates that  
 9  
 the prediction results based on data  $B_1$  are basically the same as those based on data  $B_1 + B_2$ .  
 10  
 The figure shows the prediction results based on data  $B_1$  (red number) and the prediction results  
 11  
 based on data  $B_1 + B_2$  (black number) for each EV at 0 and 120000 km, respectively. The SOH  
 12  
 of each EV is still about 85% when it reaches 120000 km.  
 13

In order to verify the capacity estimation accuracy of the method, 4 EVs are randomly  
 14  
 selected to test their capacities in field from 100 EVs provided by data source B. To be general,  
 15  
 the sampled EV are labelled as: V1, V2, V3, V4. The test time is several weeks after data  $B_2$  is  
 16  
 obtained, and the basic information of the sampled EVs is shown in Table 2.  
 17

**Table 2**  
 Basic Information of the EVs

Vehicle Number	Initial date	Initial mileage ( km )
V1	2017.12.08	130
V2	2017.12.08	92
V3	2017.12.08	64
V4	2017.12.08	66

The capacity prediction results of 4 EVs are shown in Fig. 7. The ordinate is the capacity, and  
 56  
 the abscissa is the mileage. The blue points represent the capacity estimation results ( $C_E(B_1)$ )

1 obtained based on data  $B_1$ . The red prediction curve is obtained by fitting  $C_E(B_1)$  based on  
2 Arrhenius empirical aging model. Red points represent the capacities at 0 and 120,000 km based  
3 on data  $B_1$  predictions. Brown vertical line is the location of the capacity test and the blue  
4 vertical line is the mileage of data  $B_1$ . The green points represent the capacity estimation results  
5 ( $C_E(B_2)$ ) based on data  $B_2$ , and the green vertical line is the mileage of data  $B_2$ . The black  
6 dotted line is the prediction curve based on data  $B_1 + B_2$ . Black points represent the capacities  
7 at 0 and 120,000 km based on data  $B_1 + B_2$  predictions.  
8  
9  
10  
11  
12  
13  
14  
15  
16  
17

18 For the capacity prediction results based on data  $B_1 + B_2$ , the mileages of V2 and V4 in  
19 the capacity test are close to those of the last capacity estimation respectively, which can be  
20 regarded as the verification of the capacity estimation results. The mileages of V1 and V3 in the  
21 capacity test are far away from the last capacity estimation respectively, so the results should be  
22 regarded as the prediction results. The capacity prediction results based on data  $B_1$  are very  
23 similar to the capacity prediction results based on data  $B_1 + B_2$ . For the prediction results based  
24 on data  $B_1$ , there is a prediction length of about 40000 km from the last capacity estimation to  
25 the capacity test. Table 3 shows the capacity prediction results and errors of 4 EVs. It can be seen  
26 that the errors are less than 4% no matter the prediction results based on data  $B_1$  or the  
27 prediction results based on data  $B_1 + B_2$ . The error sources may include prediction model and  
28 capacity estimation method, but on the whole, the method has a good capacity prediction accuracy  
29 and can be used for capacity estimation and life prediction on the cloud.  
30  
31  
32  
33  
34  
35  
36  
37  
38  
39  
40  
41  
42  
43  
44  
45  
46  
47  
48  
49  
50  
51  
52  
53  
54  
55  
56  
57  
58  
59  
60  
61  
62  
63  
64  
65

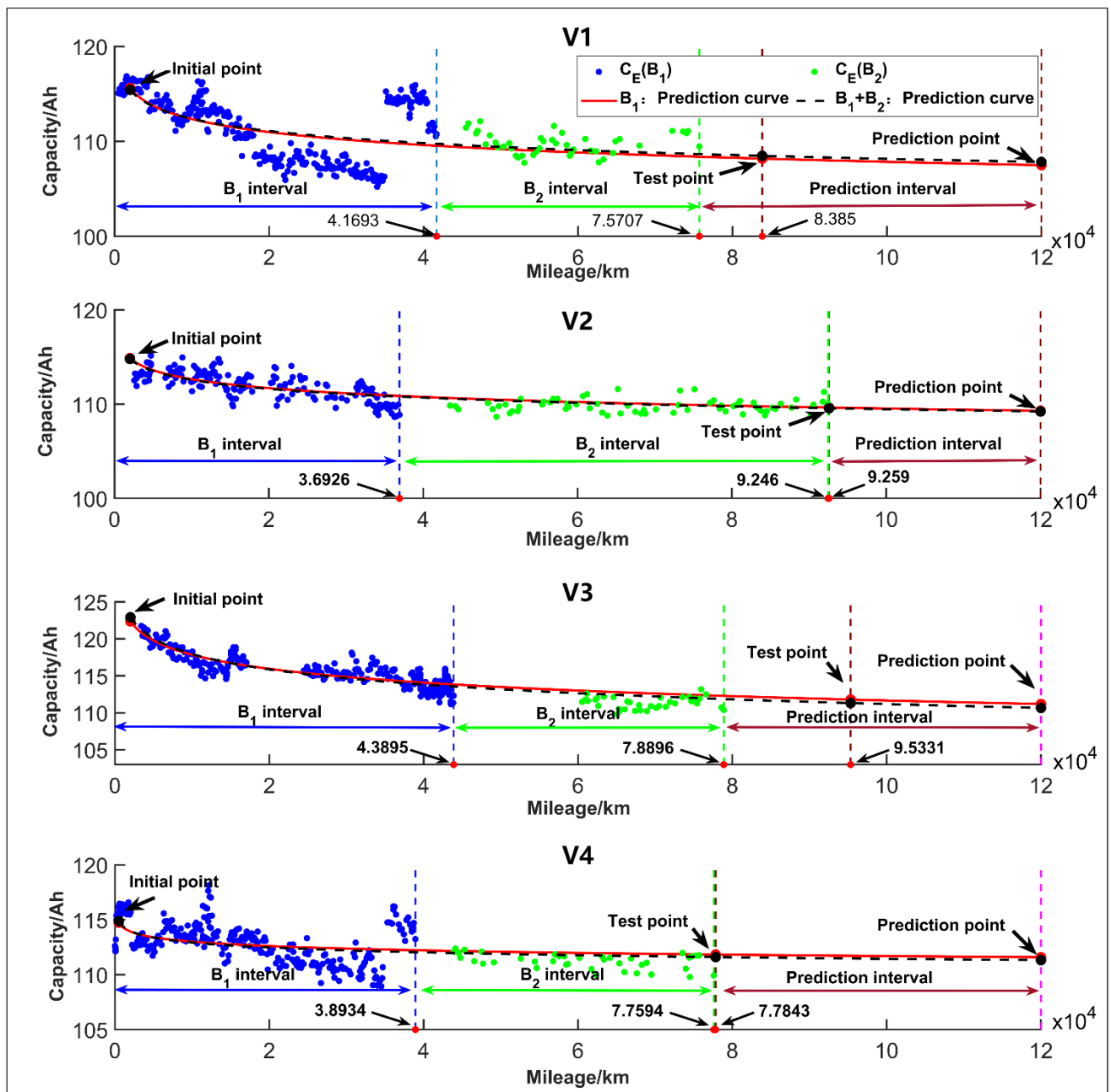


Fig. 7 Capacity prediction results of four sampled EVs

Table 3

Capacity prediction results and errors of four sampled EVs

Number	Test Time	Mileage ( km )	Test Capacity ( Ah )	Prediction		Prediction	
				Capacity : $B_1$ ( Ah )	Error ( % )	Capacity : $B_1 + B_2$ ( Ah )	Error ( % )
V1	2019.4.10	83850	109	108.18	0.75	108.47	0.49
V2	2019.4.10	92590	106	109.63	3.42	109.56	3.36
V3	2019.4.10	95331	108	111.79	3.51	111.32	3.07

#### 4.3 Results of internal resistance estimation and prediction

One EV from data source B is randomly selected for internal resistance estimation. The EV has been running for 201 days, and the temperature data during operation is shown in Fig. 8(a). The maximum temperature difference during the operation of the EV is 34°C. Fig. 8(b) is the estimation result of the internal resistance. The battery pack in the EV contains 85 cells. The points of the same color in the figure represent the internal resistance of the same cell. The blue cross points represent the average value ( $r_m$ ) of the internal resistance for 85 cells. Generally speaking, the internal resistance of a battery increases with cycles. Due to the influence of the temperature change, the internal resistance  $r_m$  in the figure shows a decrease trend with time, which is not in line with the aging law of the internal resistance. So it is necessary to modify the estimated results according to the temperature data. Based on the relationship between temperature and internal resistance shown in Fig. 2 (c),  $r_m$  is further corrected to be  $r_T$  based on the temperature data. The yellow triangles in Fig. 8(b) represent  $r_T$ . After the temperature correction,  $r_T$  increases slightly with the use of time, and the overall change is stable, which is in line with the change law of internal resistance.

Although  $r_T$  in Fig. 8(b) can reflect the change trend of the internal resistance,  $r_T$  still has strong divergence due to the complexity of cloud data, the influence of temperature, current and other variables. So we further use KF+FL algorithm to optimize  $r_T$ . In Fig. 8(c), the yellow triangles represent  $r_T$ , and the black circular points represent the results of optimizing  $r_T$  with KF + FL algorithm. The initial values of the KF+FL algorithm are as follows:

$$\hat{x}_0 = 4.5 \times 10^{-4} \Omega, P_0 = 1, Q = 0.03^2, R$$

$R$  is controlled in real time by the FL algorithm as introduced in section 3.3. The estimation results show that although there are some large estimation errors in  $r_T$ , the real-time control of  $r_T$  weight by FL algorithm can make the

estimation results converge to the real trend of the internal resistance. The blue line represents the  
predicted curve of the internal resistance, and the green point represents the predicted internal  
resistance on the 400th day. From the internal resistance estimation and prediction results, the  
internal resistance estimation results obtained by this method converge and conform to the trend of  
battery internal resistance changes, which can be used for internal resistance estimation and  
prediction on the cloud.

1  
2  
3  
4  
5  
6  
7  
8  
9  
10  
11  
12  
13  
14  
15  
16  
17  
18  
19  
20  
21  
22  
23  
24  
25  
26  
27  
28  
29  
30  
31  
32  
33  
34  
35  
36  
37  
38  
39  
40  
41  
42  
43  
44  
45  
46  
47  
48  
49  
50  
51  
52  
53  
54  
55  
56  
57  
58  
59  
60  
61  
62  
63  
64  
65

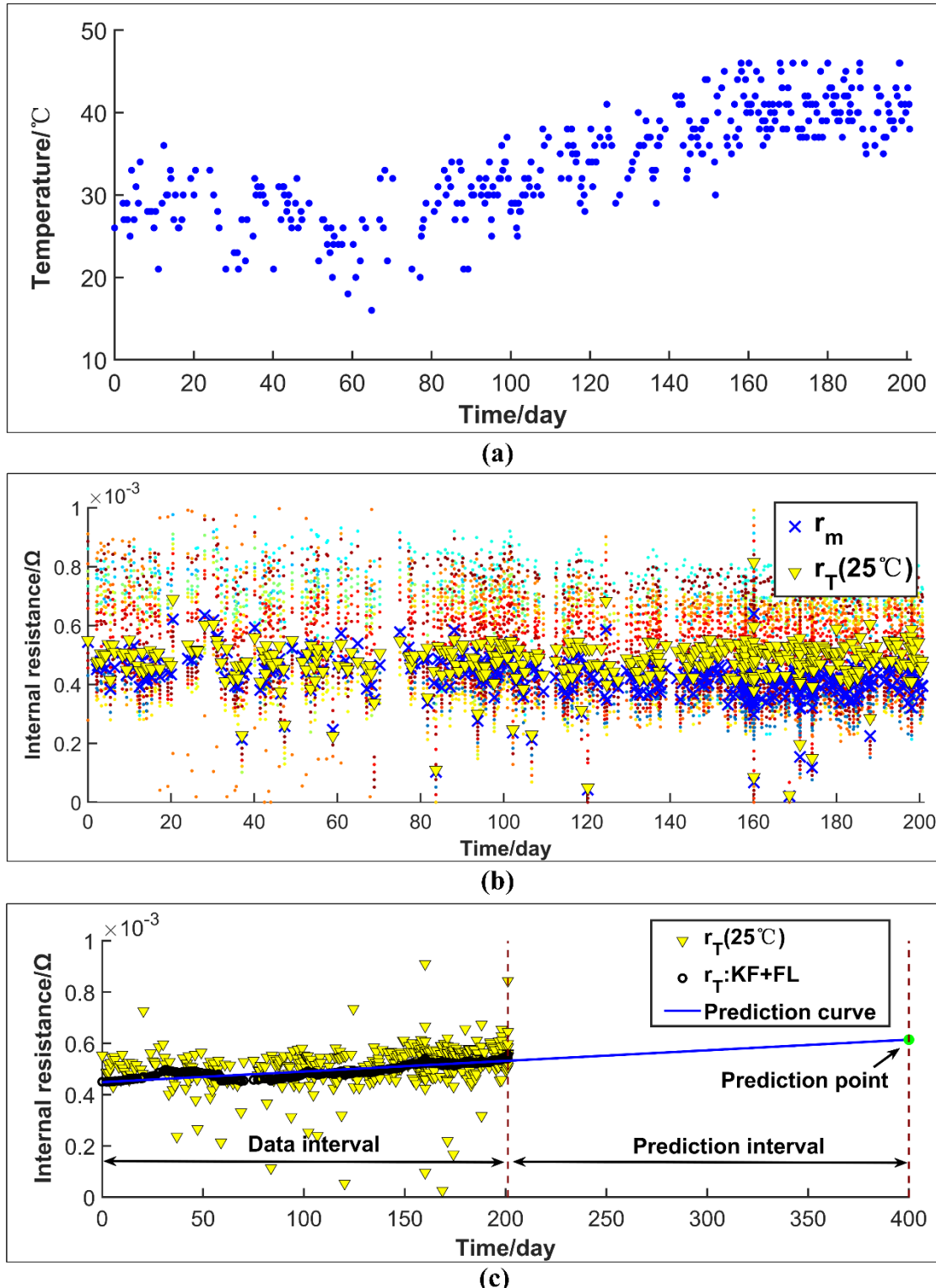


Fig. 8 (a) Temperature data (b) Internal resistance estimation results (c) Internal resistance prediction results

## 5. Conclusion

To evaluate the safety and life-cycle of EVs, automobile companies usually retain the driving data of EVs on the cloud for monitoring and management. Because the charging data are stable

1 compared to the dynamic driving condition, we propose a new battery life estimation method  
2  
3 based on the charging cloud data for EVs. Battery life estimation includes capacity estimation and  
4  
5 internal resistance estimation.  
6  
7

8 Firstly, the capacity estimation method of EV battery pack is discussed. The data on the cloud  
9 of EVs are processed and the capacity is estimated using the ampere hour integral method. Then,  
10  
11 the estimation results are modified according to the temperature data. Finally, the capacity of  
12  
13 battery pack is predicted based on the Arrhenius empirical aging model.  
14  
15  
16

17 The capacity is directly estimated by the ampere hour integral method using a large amount  
18 of historical charging data. The estimation results are then modified based on the temperature data  
19 to obtain the preliminary capacity estimation results. The KF + FL algorithm is used to optimize  
20  
21 the capacity estimation results. Based on the capacity estimation results, the battery life is finally  
22 predicted by the Arrhenius empirical aging model. For the estimation and prediction of internal  
23  
24 resistance, the sudden changes of voltage and current in the multi-stage charging data are used to  
25 estimate the internal resistance of the battery pack. The internal resistance prediction is achieved  
26  
27 using a similar process to the capacity prediction.  
28  
29  
30  
31  
32  
33  
34  
35  
36  
37  
38  
39  
40  
41

42 Considering the influence of temperature on the estimation results of capacity and internal  
43  
44 resistance, the estimation results are modified according to the temperature data, so that the  
45 estimation results of capacity and internal resistance are more consistent with the true change of  
46  
47 power battery. Besides, as large noises are unavoidable after the preliminary estimation, the FL  
48  
49 algorithm is used to control the observation noise of the KF algorithm in real time to make the  
50 estimation results converge to the true trend.  
51  
52  
53  
54  
55  
56  
57  
58

59 A total of 147 vehicle data provided by two data sources are used to verify the proposed  
60  
61  
62  
63  
64  
65

method. The results show that the estimation results of the capacity and internal resistance obtained by this method gradually converge to the true trend. The maximum estimation error of the capacity verified by the sampled real EVs is less than 4%. Based on the current cloud data, this estimation method can accurately estimate the capacity of the power battery in EVs and realize the life prediction.

## Acknowledge

This research is supported by the International Science & Technology Cooperation of China under 2019YFE0100200, National Natural Science Foundation of China (NSFC) under the Grant number of 51877138, Shanghai Science and Technology Development Fund 19QA1406200 and the Science and Technology Foundation of State Grid Corporation of China (SGCC) under the contract number of DG71-19-024. The authors appreciate the data support from Shanghai Electric Vehicle Public Data Collecting, Monitoring and Research Center (SHEVDC).

## Reference

- [1] X Han, M Ouyang, L Lu, Y Zheng, et al. J Power Sources 2014; 251:38-54.
- [2] Y Zheng, L Lu, X Han, M Ouyang, et al. J Power Sources 2013; 226:33-41.
- [3] X Han, L Lu, Y Zheng, et al. eTransportation 2019. doi: <https://doi.org/10.1016/j.etran.2019.100005>.
- [4] J Vetter, P Novak, M Wagner. J Power Sources 2009; 147:269-281.
- [5] Y Zheng, C Qin, X Lai, X Han, Y Xie. Appl Energy 2019; 251:113327.
- [6] Y Zou, X Hu, H Ma, et al. J Power Sources 2015; 273:793-803.
- [7] D Liu, Y Luo, J Liu, et al. Neural Computing and Applications 2014; 25: 557. doi: <https://doi.org/10.1007/s00521-013-1520-x>.
- [8] X Lai, C Qin, Y Zheng, et al. Automotive Engineering 2019; 41:1-6.
- [9] W He, N Williard, M Osterman, M Pecht. J Power Sources 2011; 196: 10314-10321.
- [10] D Wang, F Yang, K Tsui, Q Zhou, S Bae. IEEE Transactions on Instrumentation and Measurement 2016; 65:1282-1291.
- [11] Y Xing, E Ma, K Tsui, M Pecht. Microelectronics Reliability 2013; 53: 811-820.
- [12] G Ma, Y Zhang, C Cheng, et al. Appl Energy 2019. doi: <https://doi.org/10.1016/j.apenergy.2019.113626>.
- [13] D Andre, M Meiler, K Steiner, et al. II: Modelling. J Power Sources 2011; 196:5349-5356.
- [14] W Waag, C Fleischer, D Sauer. J Power Sources 2014; 258:321-339.
- [15] G Prasad, C Rahn. J Power Sources 2013; 232:79-85.
- [16] J Remmlinger, M Buchholz, M Meiler, et al. J Power Sources 2011; 196:5357-5363.
- [17] D Andre, A Nuhic, T Soczka-Guth, et al. Engineering Applications of Artificial Intelligence 2013; 26:951-961.
- [18] S Li, H He, J Li. Appl Energy 2019; 242:1259-1279.
- [19] Y Tao, M Huang, Y Chen, L Yang, Energy (2020), doi: <https://doi.org/10.1016/j.energy.2019.116806>.
- [20] M Gennaro, et al. Case Studies on Transport Policy (2019), doi: <https://doi.org/10.1016/j.cstp.2019.11.005>.
- [21] Z Guo, X Qiu, G Hou, et al. J Power Sources 2014; 249:457-462.
- [22] X Meng, Z Wang. High Technology Letters 2010; 16:13-17.
- [23] D Liu, H Wang, Y Peng, W Xie, H Liao. Energies 2013; 6:3654–3668.
- [24] S Tang, C Yu, X Wang, X Guo, X Si. Energies 2014; 7:520–547.
- [25] H Tian, P Qin, K Li, H Wang. Control and Decision. doi: <https://doi.org/10.13195/j.kzyjc.2019.0764>.
- [26] M Einhorn, F Conte, C Kral, et al. IEEE Transactions on Industry Applications 2012; 48:736-741.

- [27] L Jin, Z Sun, Z Liu, et al. *Automotive Engineering* 2019; 41:591-606.
- [28] S Lalouni, D Rekioua, T Rekioua, E Matagne, *J Power Sources* 2009; 193:899-907.
- [29] X Han. BeiJing: Tsinghua University, 2014.
- [30] L Bloom, B Cole, J Sohn, et al. *J Power Sources* 2001; 101:238-247.
- [31] S Zhang, K Xu, T Jow. *Electrochimica Acta* 2014; 49:1057-1061.s
- [32] Y Lu. *J Power Sources* 2017; 41:702-704.
- [33] X Wei, W Xu, D Shen. *J Power Sources* 2009; 33:217-220.

**Table(s) - provided separately****Table 1**

Basic Information of Real Vehicle Data

<b>Source</b>	<b>Number of data</b>	<b>Sampling days</b>
A	47	~345
B	100	~469

**Table 2**

Basic Information of the EVs

<b>Vehicle Number</b>	<b>Initial date</b>	<b>Initial mileage ( km )</b>
V1	2017.12.08	130
V2	2017.12.08	92
V3	2017.12.08	64
V4	2017.12.08	66

**Table 3**

Capacity prediction results and errors of four sampled EVs

Number	Test Time	Mileage ( km )	Test Capacity ( Ah )	Prediction		Prediction	
				Capacity : $B_1$ ( Ah )	Error (%)	Capacity : $B_1 + B_2$ ( Ah )	Error (%)
V1	2019.4.10	83850	109	108.18	0.75	108.47	0.49
V2	2019.4.10	92590	106	109.63	3.42	109.56	3.36
V3	2019.4.10	95331	108	111.79	3.51	111.32	3.07
V4	2019.4.10	77843	108	111.83	3.55	111.6	3.33

# Figure(s) - provided separately

[Click here to download Figure\(s\) - provided separately: Figure.docx](#)

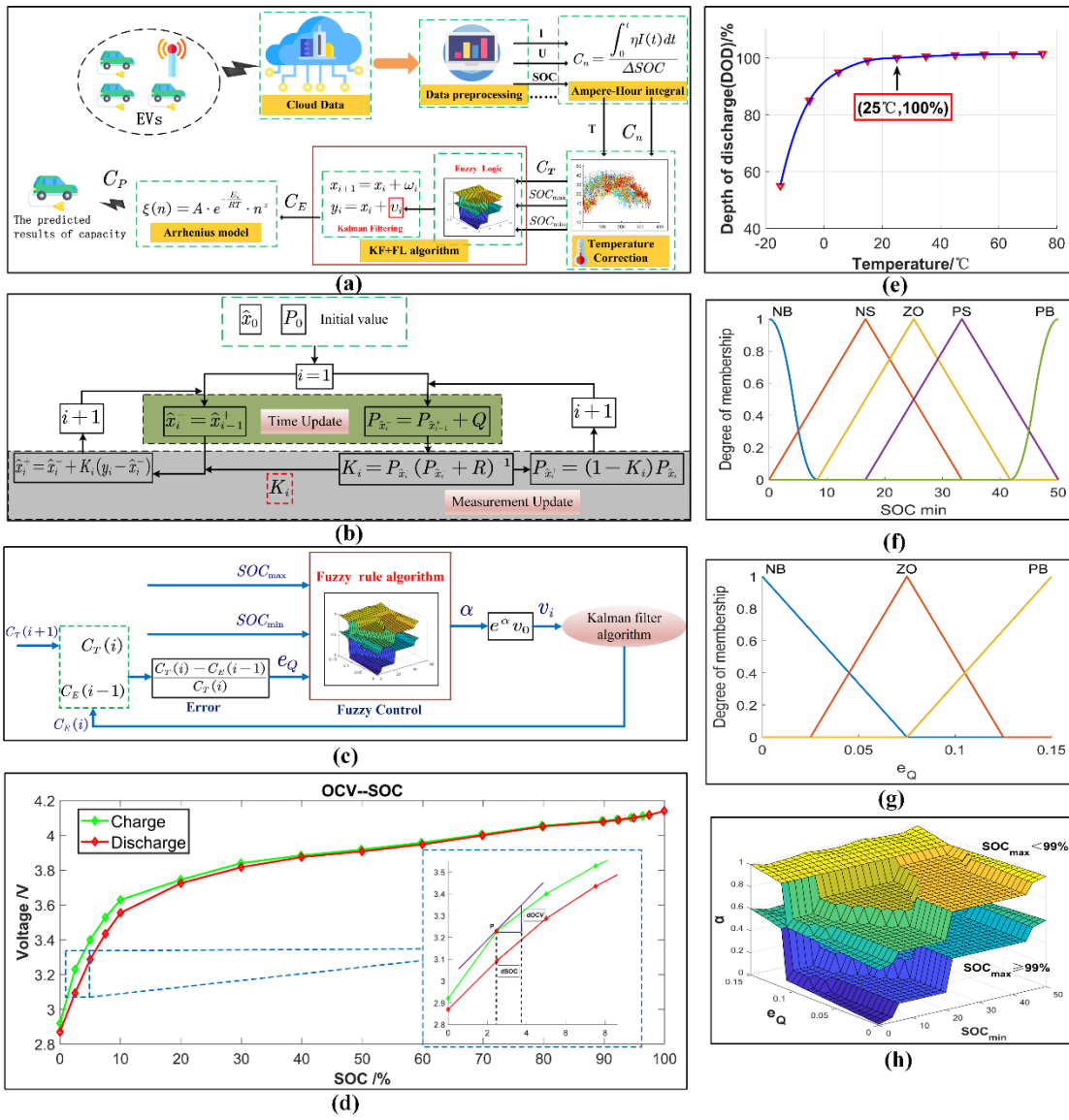


Fig. 1(a)Capacity estimation process (b) KF algorithm process (c)KF+FL algorithm process (d)OCV-SOC curve (e)Relationship between depth of discharge and temperature (f) membership function (g) membership function (h)Capacity fuzzy rule graph

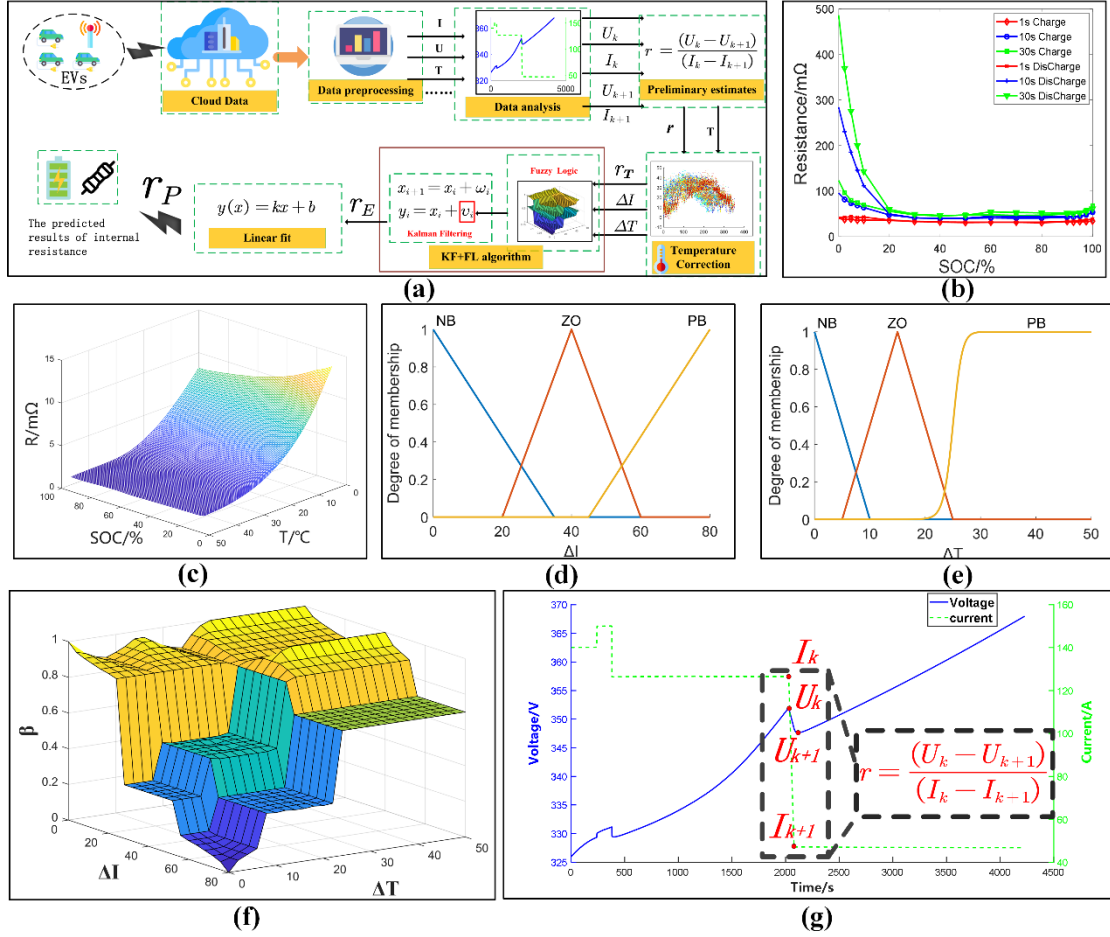


Fig. 2 (a)Internal resistance estimation process (b)Relationship between internal resistance and SOC under different charging and discharging pulses (c)Relationship between internal resistance, temperature and SOC (d) membership function (e) membership function (f)internal resistance fuzzy rule graph (g)Charging voltage and current

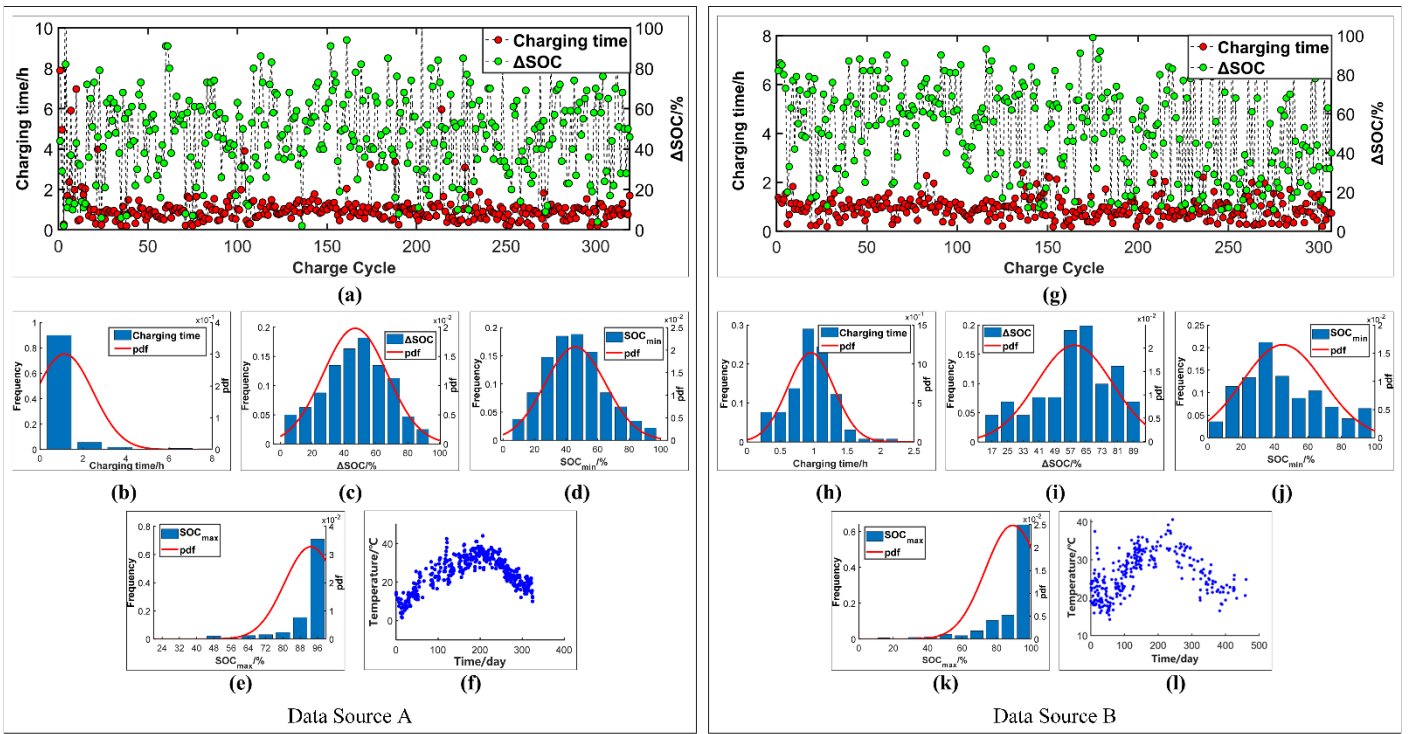
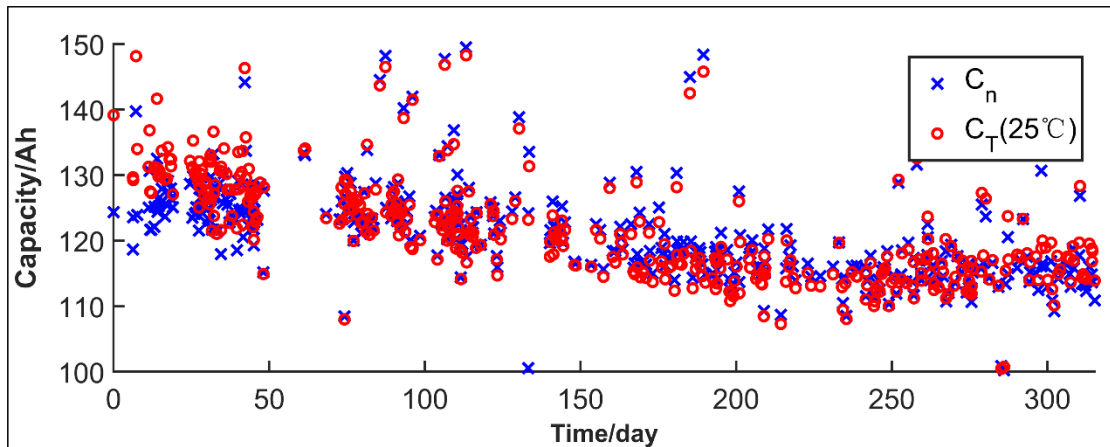
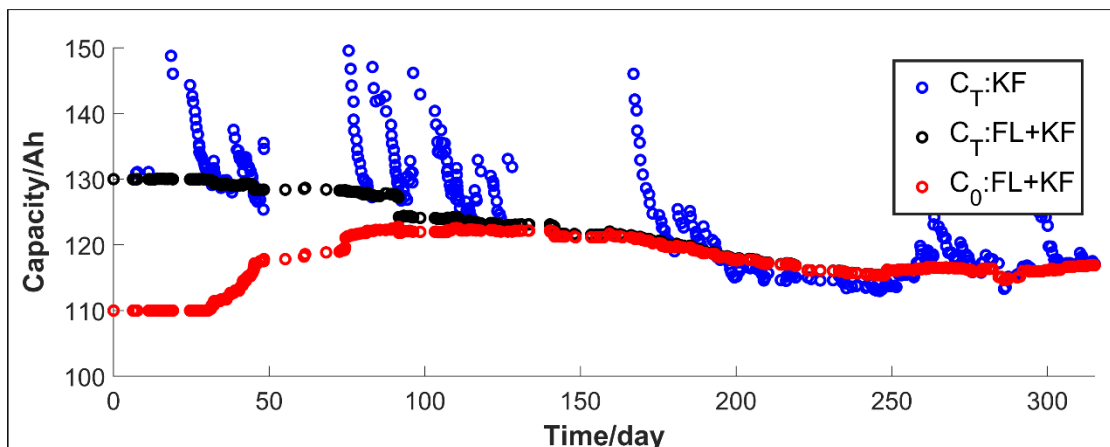


Fig. 3 (a) and (g) charging time and depth of charge  
(b) and (h) frequency distribution histogram of the charging  
(c) and (i) frequency distribution histogram of  
(d) and (j) frequency distribution histogram of  
(e) and  
(f) and (l) Temperature data



(a)



(b)

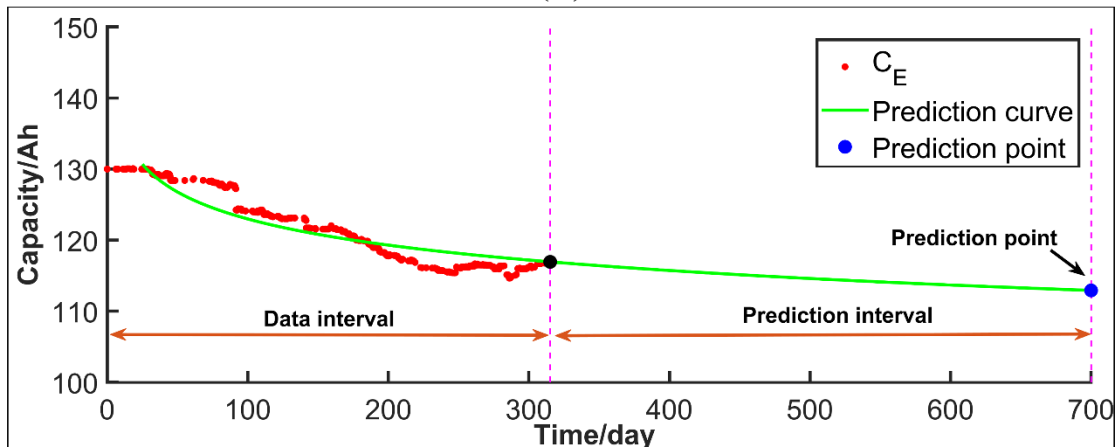


Fig. 4 (a) Preliminary capacity estimation results (b)Capacity estimation results of KF Algorithm and KF + FL Algorithm (c) Capacity Prediction results

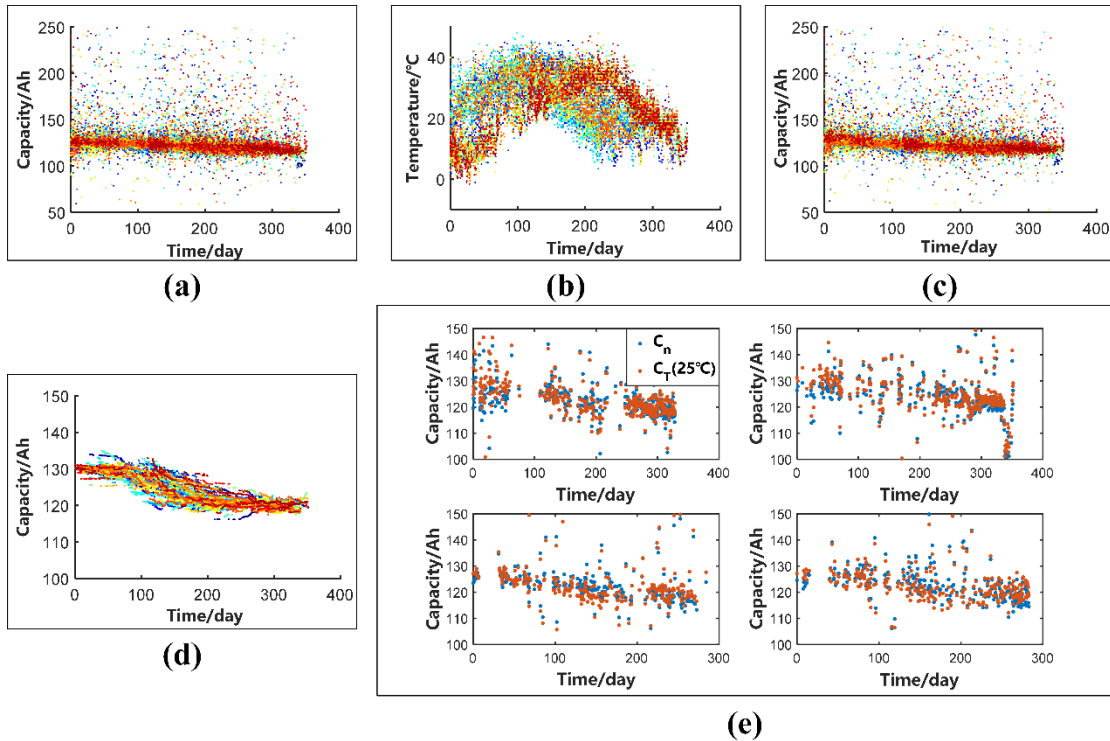


Fig. 5 All EVs from data source A: (a) Preliminary capacity estimation results (b) Temperature data (c) Temperature correction results (d) Capacity estimation results of KF + FL Algorithm (e) Single EV temperature correction results

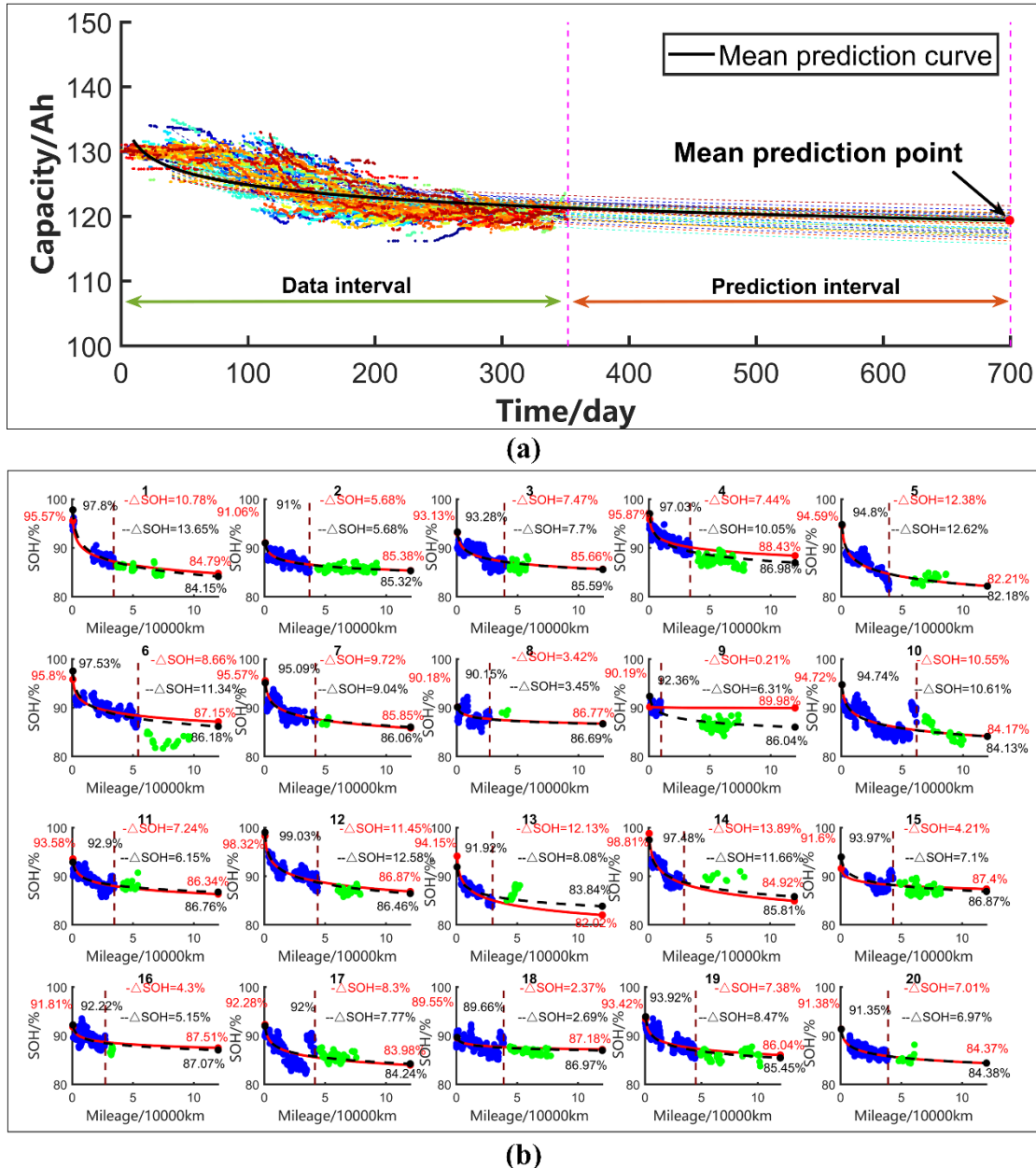


Fig. 6 (a)Capacity prediction results of 47 EVs (b) Model free SOH estimation and empirical life model SOH prediction based on EV cloud data

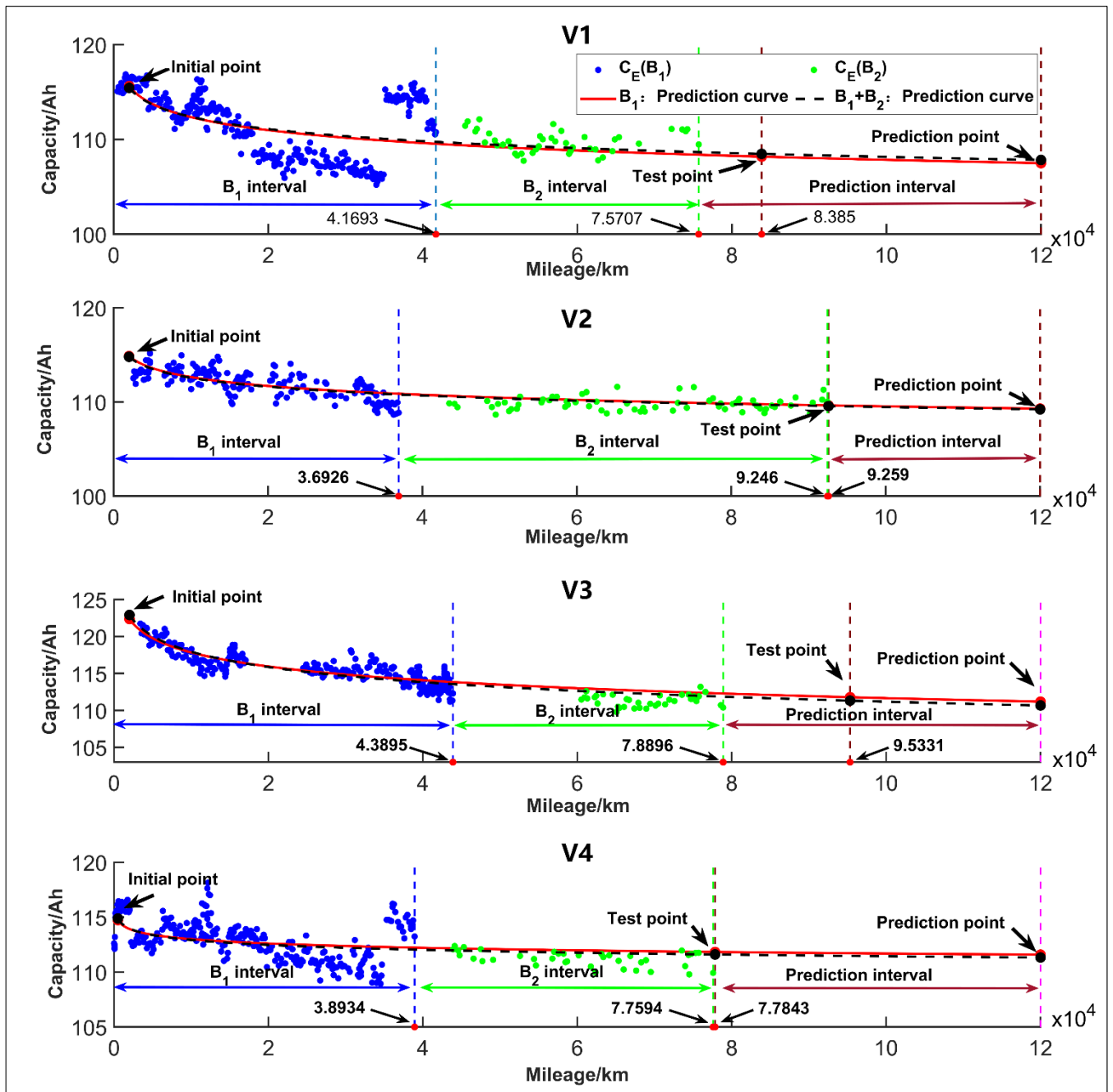


Fig. 7 Capacity prediction results of four sampled EVs

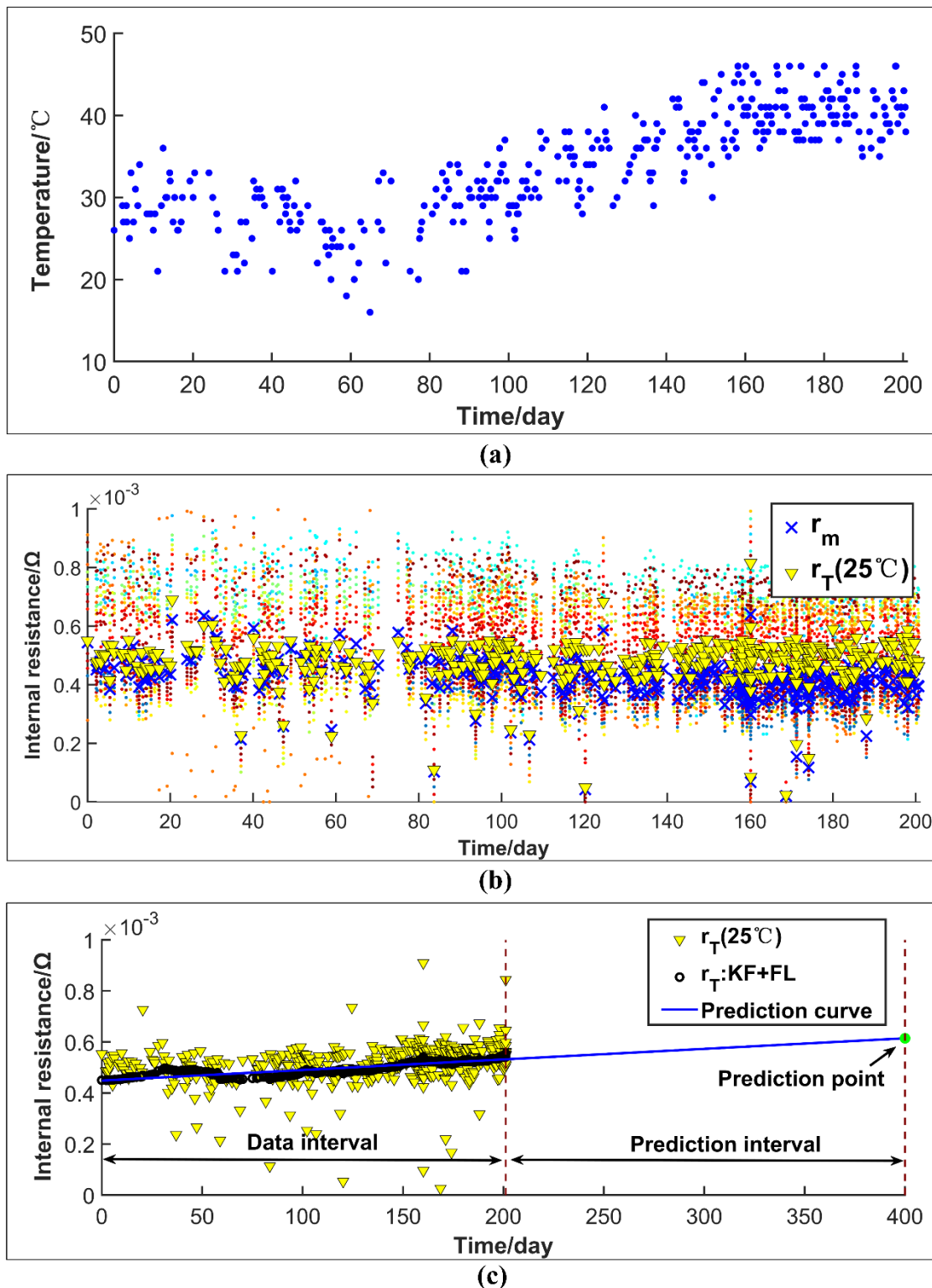


Fig. 8 (a)Temperature data (b)Internal resistance estimation results (c)Internal resistance prediction results

Fig. 1(a)Capacity estimation process (b) KF algorithm process (c)KF+FL algorithm process (d)OCV-SOC curve  
(e)Relationship between depth of discharge and temperature (f) membership function (g) membership function  
(h)Capacity fuzzy rule graph

Fig. 2 (a)Internal resistance estimation process (b)Relationship between internal resistance and SOC under different charging and discharging pulses (c)Relationship between internal resistance, temperature and SOC (d) membership function (e) membership function (f)internal resistance fuzzy rule graph (g)Charging voltage and current

Fig. 3 (a) and (g)charging time and depth of charge (b) and (h)frequency distribution histogram of the charging time (c) and (i)frequency distribution histogram of (d) and (j)frequency distribution histogram of (e) and (k)frequency distribution histogram of (f) and (l)Temperature data

Fig. 4 (a) Preliminary capacity estimation results (b)Capacity estimation results of KF Algorithm and KF + FL Algorithm (c) Capacity Prediction results

Fig. 5 All EVs from data source A: (a) Preliminary capacity estimation results (b) Temperature data (c) Temperature correction results (d) Capacity estimation results of KF + FL Algorithm (e) Single EV temperature correction results

Fig. 6 (a)Capacity prediction results of 47 EVs (b) Model free SOH estimation and empirical life model SOH prediction based on EV cloud data

Fig. 7 Capacity prediction results of four sampled EVs

Fig. 8 (a)Temperature data (b)Internal resistance estimation results (c)Internal resistance prediction results

**Table 1**

Basic Information of Real Vehicle Data

**Table 2**

Basic Information of the EVs

**Table 3**

Capacity prediction results and errors of four sampled EVs

- A method for life estimation and prediction of electric vehicle power battery is proposed.
- Estimated the capacity and internal resistance of electric vehicle power battery based on cloud charging data.
- The fuzzy logic is used for controlling the observed noise of the KF algorithm to make the filtering result converge.
- The capacity and internal resistance of electric vehicle power battery is predicted based on the Arrhenius empirical model and linear model, respectively.

**\*Declaration of Interest Statement**

**Declaration of interests**

The authors declare that they have no known competing financial interests or personal relationships that could have appeared to influence the work reported in this paper.

The authors declare the following financial interests/personal relationships which may be considered as potential competing interests: